Today's Outline - November 28, 2016

Today's Outline - November 28, 2016

- Presentation schedule

Today's Outline - November 28, 2016

- Presentation schedule
- Grating interferometry

Today's Outline - November 28, 2016

- Presentation schedule
- Grating interferometry
- Coherent diffraction imaging

Today's Outline - November 28, 2016

- Presentation schedule
- Grating interferometry
- Coherent diffraction imaging
- Holography

Today's Outline - November 28, 2016

- Presentation schedule
- Grating interferometry
- Coherent diffraction imaging
- Holography
- Imaging research

Today's Outline - November 28, 2016

- Presentation schedule
- Grating interferometry
- Coherent diffraction imaging
- Holography
- Imaging research

Final Exam information

Wednesday, December 7, 2016, room 213 SB

Final Exam – Session 1, 09:00-11:20

09:00 Johan Nilsson – High-energy surface x-ray diffraction for fast surface structure determination

09:20 Kathy Ho – In situ synchrotron x-ray imaging on morphological evolution of dendrites in Sn-Bi hypoeutectic alloy under electric currents

09:40 Jason Lerch – X-ray PIV measurement of deep vein blood flow in a rat

10:00 Shokoufeh Asalzadeh – Structural evolution of platinum thin films grown by atomic layer deposition

10:20 Stoichko Antonov – Visualization of a lost painting by Vincent van Gogh using synchrotron radiation based x-ray fluorescence elemental mapping

10:40 Henry Gong – Three-dimensional imaging of crystalline inclusions embedded in intact maize stalks

11:00 Runzi Cui – Spherical quartz crystals investigated with synchrotron radiation

Final Exam – Session 2, 13:00-15:40

13:00 Nicholas Goldring – Reactivity of $LiBH_4$: In situ synchrotron radiation powder x-ray diffraction study

13:20 Anthony Llodra – Imaging instantaneous electron flow with ultrafast resonant x-ray scattering

13:40 Gongxiaohui Chen – Rotation of x-ray polarization in the glitches of a silicon monochromator

14:00 Sarah Aldakheel – Synchrotron radiation diffraction enchanced imaging of chronic glomerulonephritis mode

14:20 Bo Liu – Chain stiffness of stilbene containing alternating copolymers by SAXS and SEC

14:40 Krishna Joshi – Transition elements and nucleation in glasses using x-ray absorption spectroscopy

15:00 Yang Liu – Visualization and quantification of electrochemical and mechanical degradation in Li ion batteries

15:20 Yiqing Zhang – TBD

Grating interferometry

Full field phase imaging can be achieved using an interferometric technique

Grating interferometry

Full field phase imaging can be achieved using an interferometric technique
Talbot effect: vertical grating illuminated by a plane wave

Grating interferometry

Full field phase imaging can be achieved using an interferometric technique
Talbot effect: vertical grating illuminated by a plane wave

for a vertical grating of period p_1 illuminated by a wavelength λ the transverse wave number is $k_x = 2\pi/p_1$

Grating interferometry

Full field phase imaging can be achieved using an interferometric technique
Talbot effect: vertical grating illuminated by a plane wave

for a vertical grating of period p_1 illuminated by a wavelength λ the transverse wave number is $k_x = 2\pi/p_1$

propagating the wave downstream as described previously

Grating interferometry

Full field phase imaging can be achieved using an interferometric technique
Talbot effect: vertical grating illuminated by a plane wave

for a vertical grating of period p_1 illuminated by a wavelength λ the transverse wave number is $k_x = 2\pi/p_1$

propagating the wave downstream as described previously

$\tilde{\psi}_x \sim e^{ik_x^2 z/(2k)}$

Grating interferometry

Full field phase imaging can be achieved using an interferometric technique
Talbot effect: vertical grating illuminated by a plane wave

for a vertical grating of period p_1 illuminated by a wavelength λ the transverse wave number is $k_x = 2\pi/p_1$

propagating the wave downstream as described previously

$$\tilde{\psi}_x \sim e^{ik_x^2 z/(2k)}$$
$$\sim e^{i(2\pi/p_1)^2 z/(2k)}$$

Grating interferometry

Full field phase imaging can be achieved using an interferometric technique
Talbot effect: vertical grating illuminated by a plane wave

for a vertical grating of period p_1 illuminated by a wavelength λ the transverse wave number is $k_x = 2\pi/p_1$

propagating the wave downstream as described previously

$$\tilde{\psi}_x \sim e^{ik_x^2 z/(2k)}$$
$$\sim e^{i(2\pi/p_1)^2 z/(2k)}$$
$$\sim e^{i2\pi\lambda z/(2p_1^2)}$$

Grating interferometry

Full field phase imaging can be achieved using an interferometric technique
Talbot effect: vertical grating illuminated by a plane wave

for a vertical grating of period p_1 illuminated by a wavelength λ the transverse wave number is $k_x = 2\pi/p_1$

propagating the wave downstream as described previously the repeat distance, called the Talbot distance, is given by $d_T = 2p_1^2/\lambda$

$$\begin{aligned}\tilde{\psi}_x &\sim e^{ik_x^2 z/(2k)} \\ &\sim e^{i(2\pi/p_1)^2 z/(2k)} \\ &\sim e^{i2\pi\lambda z/(2p_1^2)}\end{aligned}$$

Grating interferometry

Full field phase imaging can be achieved using an interferometric technique
Talbot effect: vertical grating illuminated by a plane wave

for a vertical grating of period p_1 illuminated by a wavelength λ the transverse wave number is $k_x = 2\pi/p_1$

propagating the wave downstream as described previously the repeat distance, called the Talbot distance, is given by $d_T = 2p_1^2/\lambda$

for $p_1 = 1\mu$m and $\lambda = 1$Å we have a Talbot distance, $d_T = 20$mm

$$\begin{aligned}\tilde{\psi}_x &\sim e^{ik_x^2 z/(2k)} \\ &\sim e^{i(2\pi/p_1)^2 z/(2k)} \\ &\sim e^{i2\pi\lambda z/(2p_1^2)}\end{aligned}$$

Grating interferometry

Full field phase imaging can be achieved using an interferometric technique
Talbot effect: vertical grating illuminated by a plane wave

for a vertical grating of period p_1 illuminated by a wavelength λ the transverse wave number is $k_x = 2\pi/p_1$

propagating the wave downstream as described previously the repeat distance, called the Talbot distance, is given by $d_T = 2p_1^2/\lambda$

for $p_1 = 1\mu$m and $\lambda = 1$Å we have a Talbot distance, $d_T = 20$mm

for an absorption grating

$$\tilde{\psi}_x \sim e^{ik_x^2 z/(2k)}$$
$$\sim e^{i(2\pi/p_1)^2 z/(2k)}$$
$$\sim e^{i2\pi\lambda z/(2p_1^2)}$$

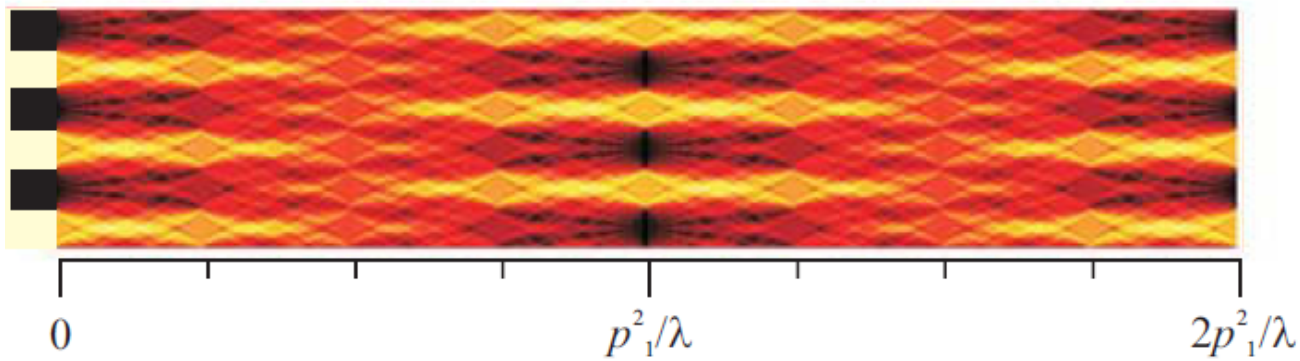

Grating interferometry

Full field phase imaging can be achieved using an interferometric technique
Talbot effect: vertical grating illuminated by a plane wave

for a vertical grating of period p_1 illuminated by a wavelength λ the transverse wave number is $k_x = 2\pi/p_1$

propagating the wave downstream as described previously the repeat distance, called the Talbot distance, is given by $d_T = 2p_1^2/\lambda$

for $p_1 = 1\mu$m and $\lambda = 1$Å we have a Talbot distance, $d_T = 20$mm

for a partial phase grating

$$\tilde{\psi}_x \sim e^{ik_x^2 z/(2k)}$$
$$\sim e^{i(2\pi/p_1)^2 z/(2k)}$$
$$\sim e^{i2\pi\lambda z/(2p_1^2)}$$

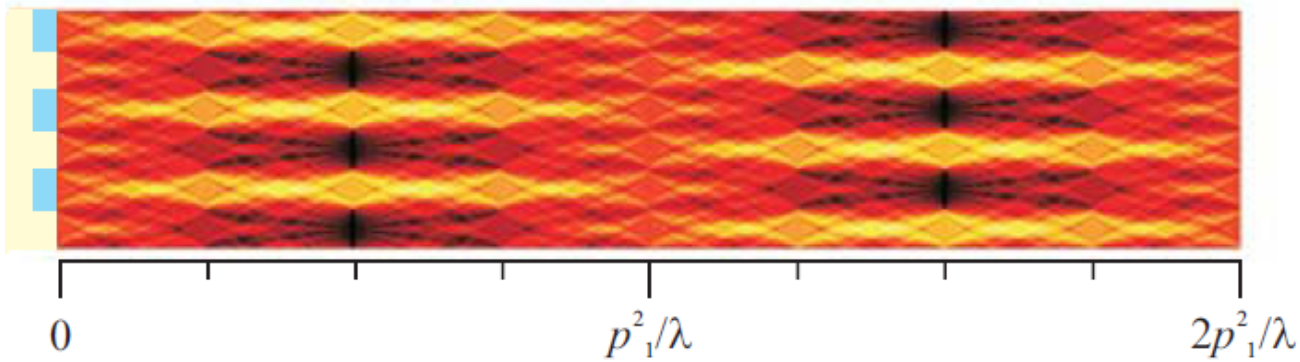

the pattern of transmission may be repeated at rational fractions of d_T

Grating interferometry

Full field phase imaging can be achieved using an interferometric technique
Talbot effect: vertical grating illuminated by a plane wave

for a vertical grating of period p_1 illuminated by a wavelength λ the transverse wave number is $k_x = 2\pi/p_1$

propagating the wave downstream as described previously the repeat distance, called the Talbot distance, is given by $d_T = 2p_1^2/\lambda$

for $p_1 = 1\mu$m and $\lambda = 1$Å we have a Talbot distance, $d_T = 20$mm

for a full π phase grating the lateral period is doubled

$$\tilde{\psi}_x \sim e^{ik_x^2 z/(2k)}$$
$$\sim e^{i(2\pi/p_1)^2 z/(2k)}$$
$$\sim e^{i2\pi\lambda z/(2p_1^2)}$$

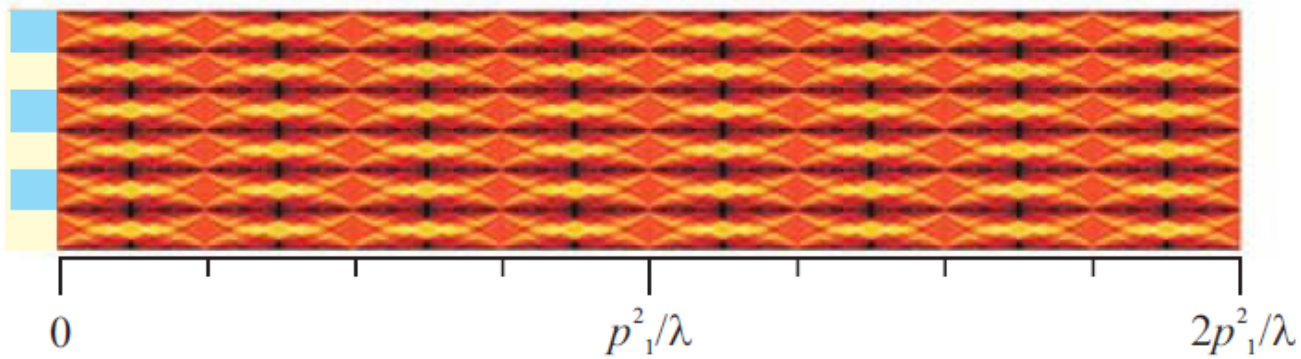

the pattern of transmission may be repeated at rational fractions of d_T

Talbot Interferometer

The Talbot interferometer consists of two gratings, a phase grating of lateral period p_1 (G1) and an absorption grating of lateral period $p_1/2$ (G2) which in combination, measure the distortion of the phase field due to the sample

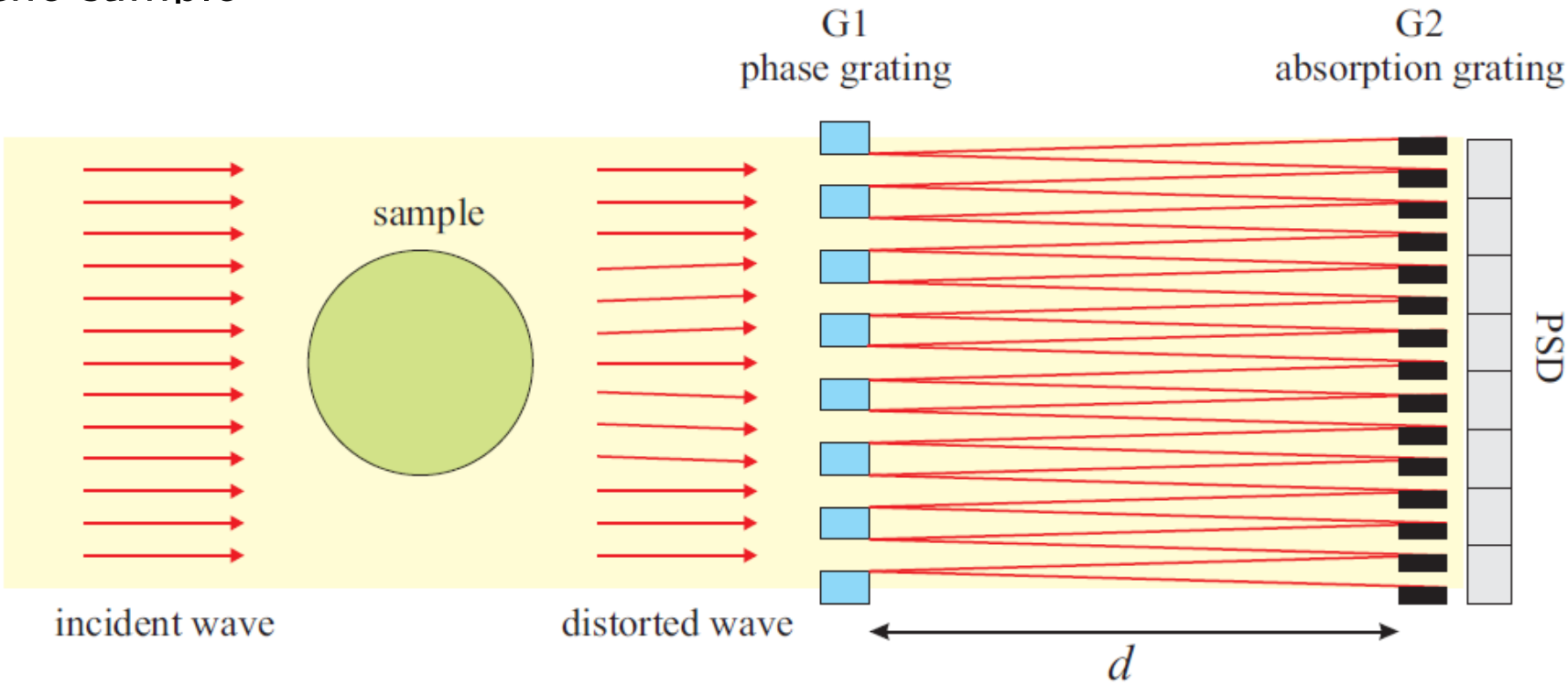

Talbot Interferometer

The Talbot interferometer consists of two gratings, a phase grating of lateral period p_1 (G1) and an absorption grating of lateral period $p_1/2$ (G2) which in combination, measure the distortion of the phase field due to the sample

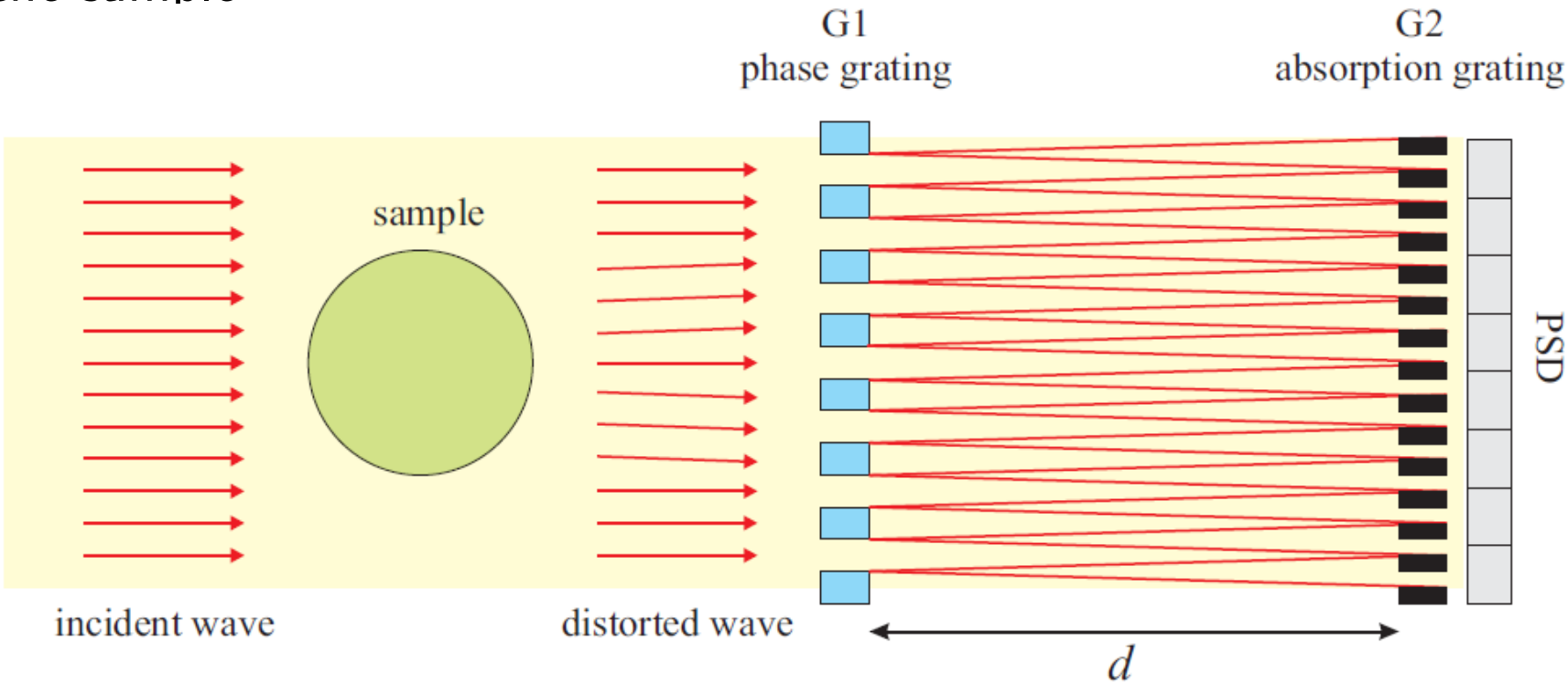

when measuring, G1 if held fixed and G2 is scanned laterally over a full period p_1

Talbot interferometer operation

With no sample in place, the pink blocks are the intensity at $d = p_1^2/8\lambda$ downstream from a $\phi = \pi$ grating

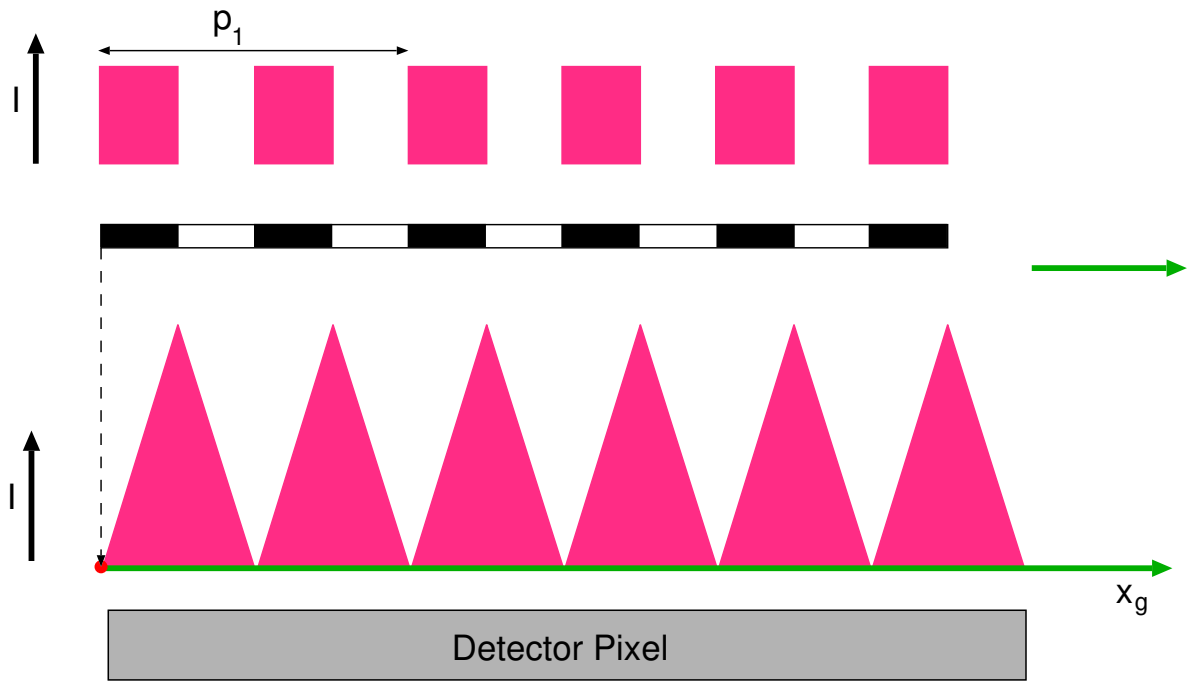

Talbot interferometer operation

With no sample in place, the pink blocks are the intensity at $d = p_1^2/8\lambda$ downstream from a $\phi = \pi$ grating

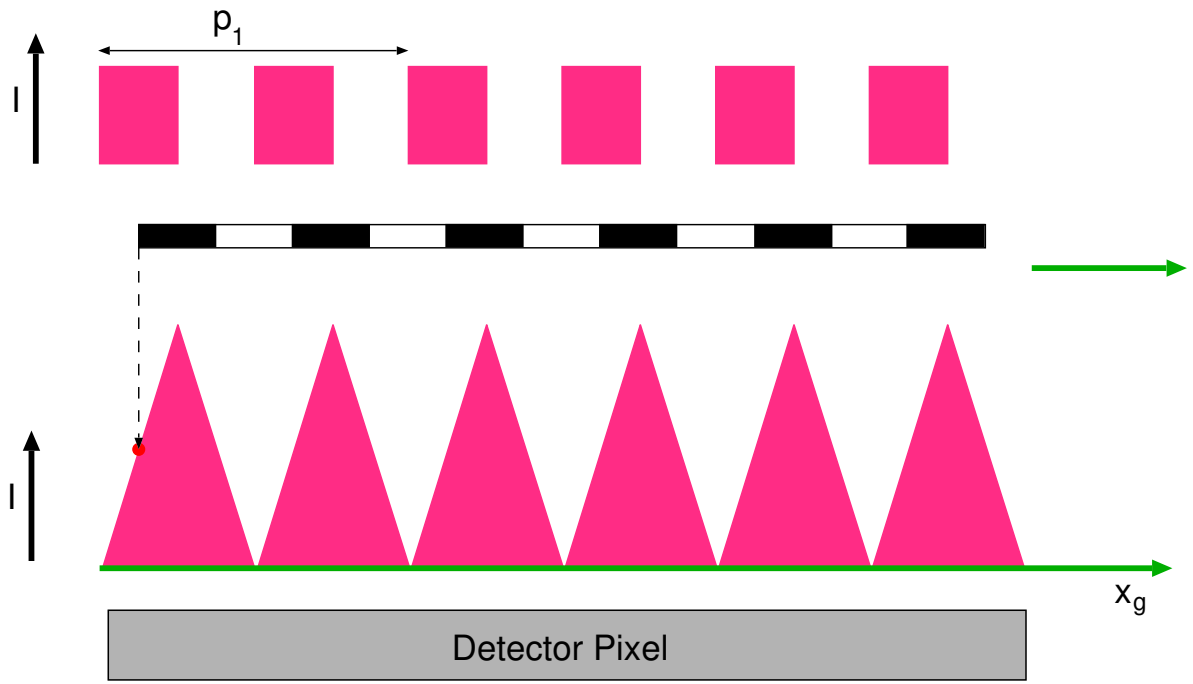

as the absorption grating, (G2) is moved laterally, the pink triagles show the ideal intensity observed at the detector as a function of x_g

Talbot interferometer operation

With no sample in place, the pink blocks are the intensity at $d = p_1^2/8\lambda$ downstream from a $\phi = \pi$ grating

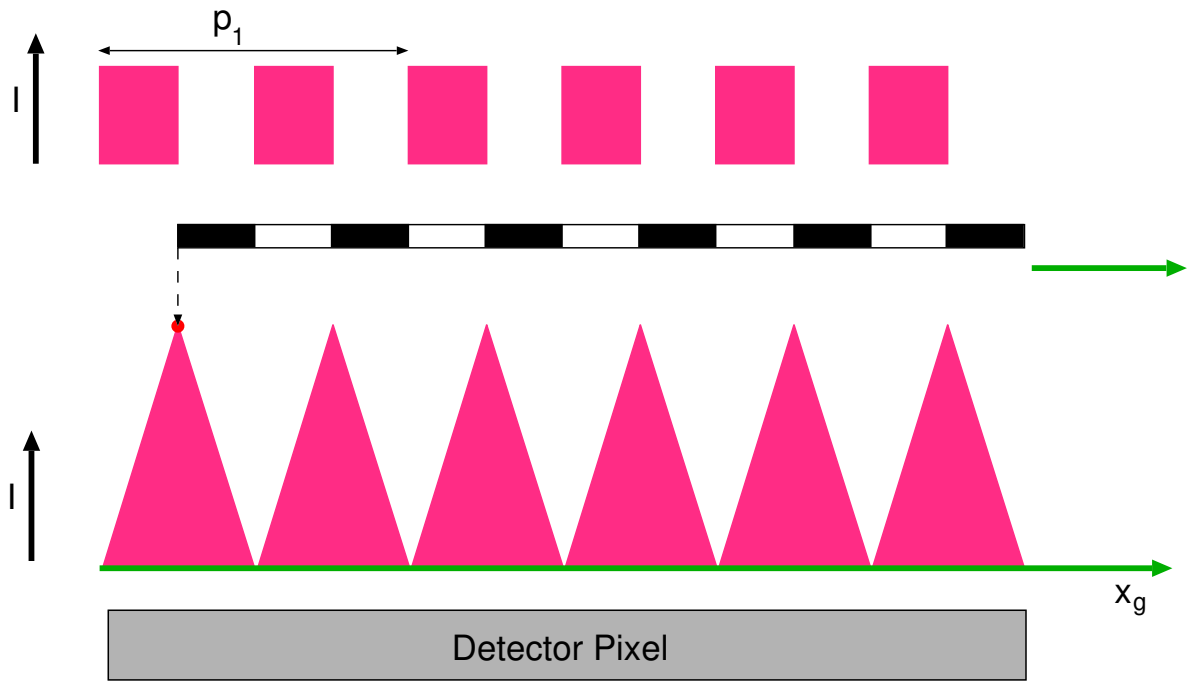

as the absorption grating, (G2) is moved laterally, the pink triagles show the ideal intensity observed at the detector as a function of x_g

Talbot interferometer operation

With no sample in place, the pink blocks are the intensity at $d = p_1^2/8\lambda$ downstream from a $\phi = \pi$ grating

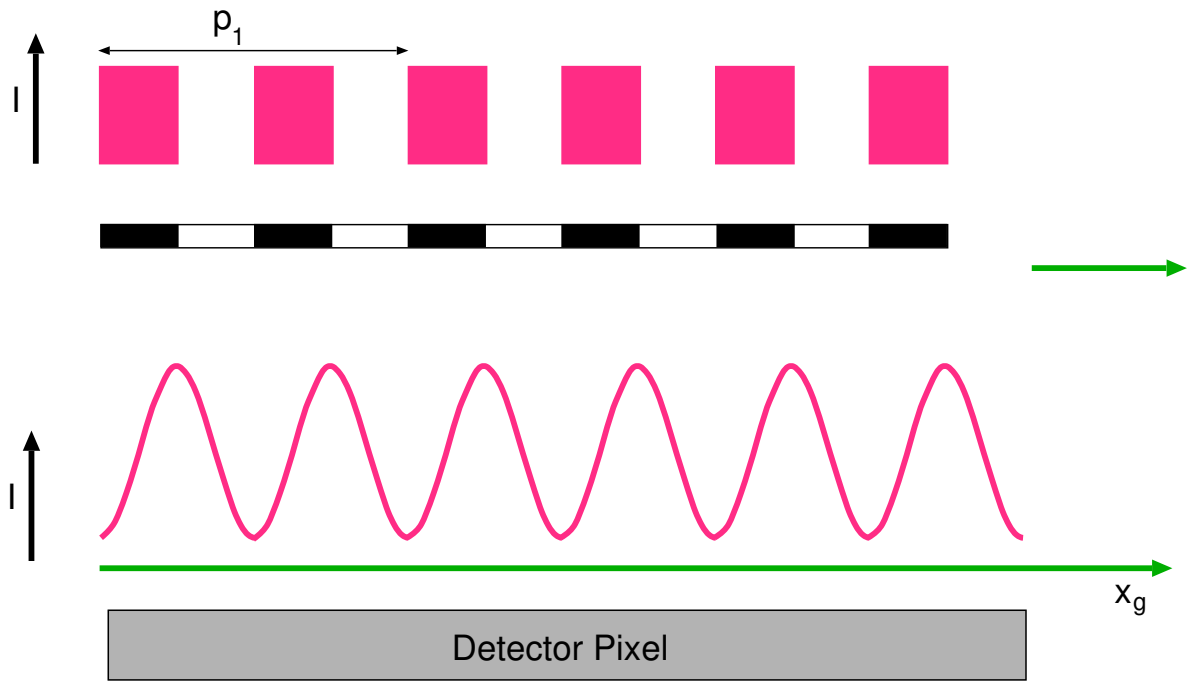

as the absorption grating, (G2) is moved laterally, the pink triagles show the ideal intensity observed at the detector as a function of x_g

the real intensity is more sinusoidal because of finite beam size

Talbot interferometer operation

With no sample in place, the pink blocks are the intensity at $d = p_1^2/8\lambda$ downstream from a $\phi = \pi$ grating

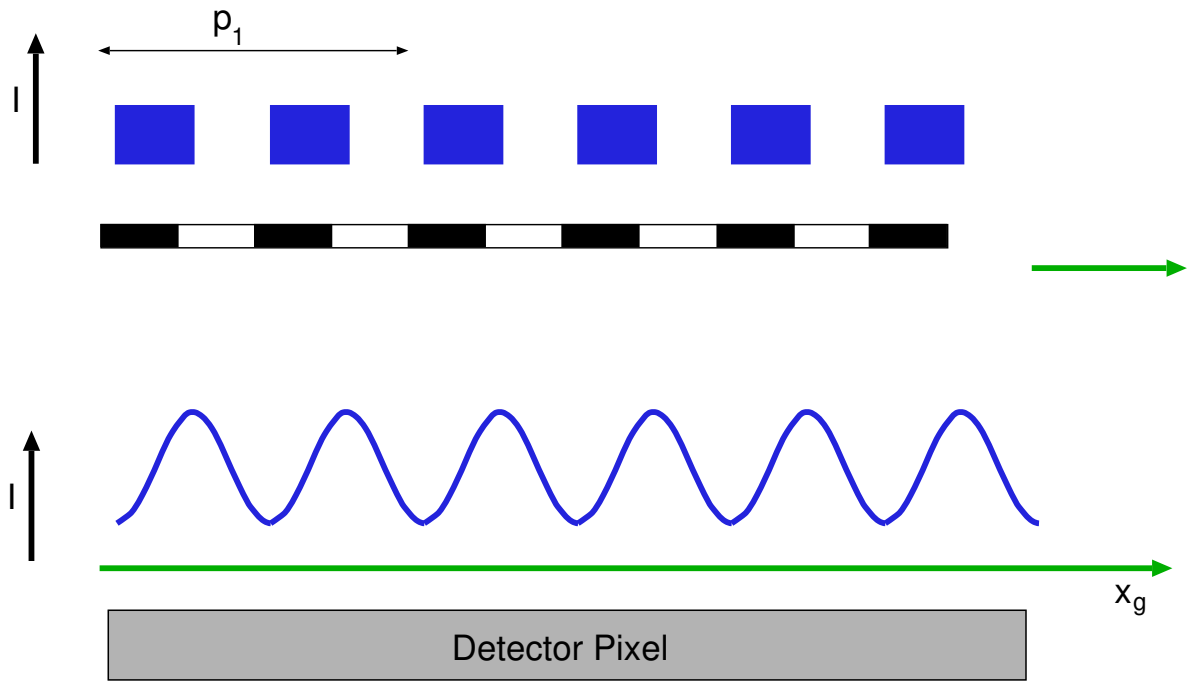

as the absorption grating, (G2) is moved laterally, the pink triagles show the ideal intensity observed at the detector as a function of x_g

the real intensity is more sinusoidal because of finite beam size

when the sample is in place the intensity is reduced and shifted by refraction to the blue blocks and curve

Talbot interferometer operation

With no sample in place, the pink blocks are the intensity at $d = p_1^2/8\lambda$ downstream from a $\phi = \pi$ grating

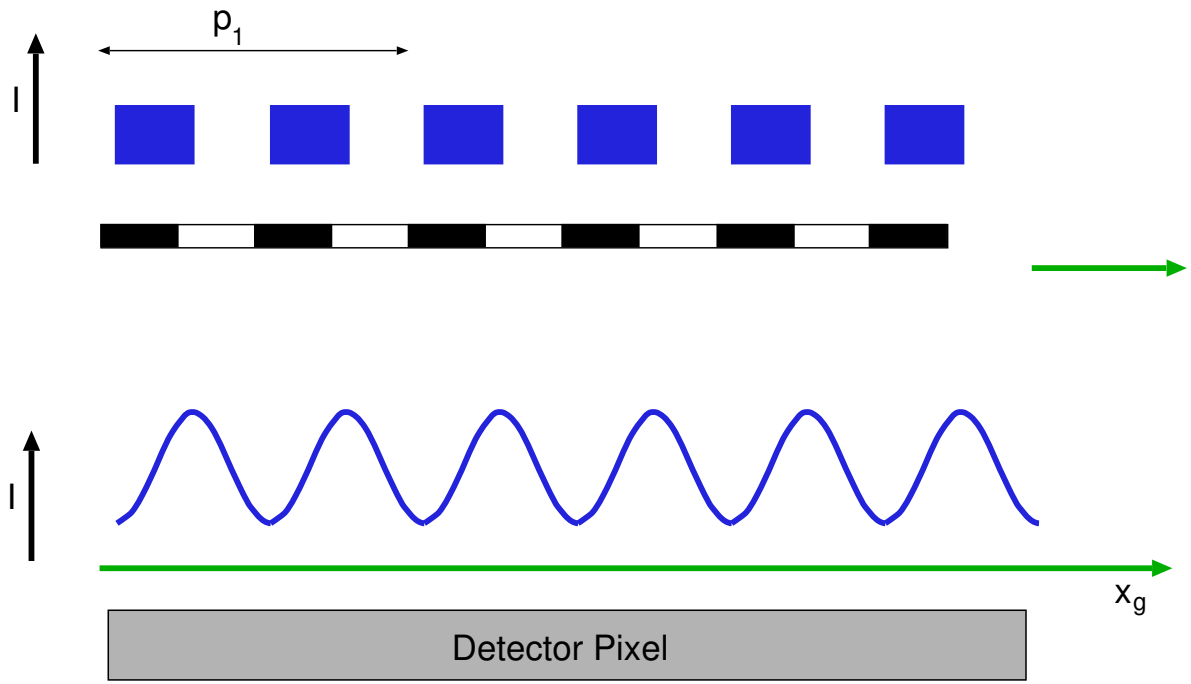

three positions of the absorption grating are all that is needed to obtain the information to produce absorption, dark field and phase contrast images

as the absorption grating, (G2) is moved laterally, the pink triagles show the ideal intensity observed at the detector as a function of x_g

the real intensity is more sinusoidal because of finite beam size

when the sample is in place the intensity is reduced and shifted by refraction to the blue blocks and curve

Visibility

We can define the visibility function as

Visibility

We can define the visibility function as

$$V = \frac{I_{max} - I_{min}}{I_{max} + I_{min}}$$

Visibility

We can define the visibility function as

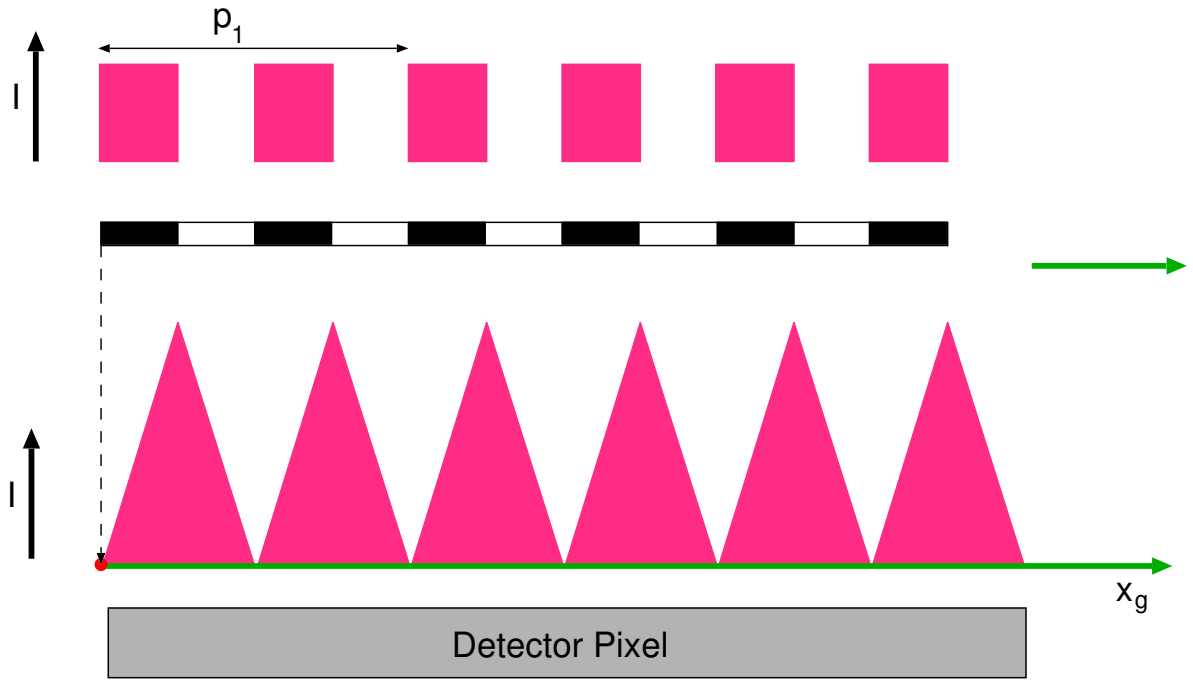

$$V = \frac{I_{max} - I_{min}}{I_{max} + I_{min}}$$

for the ideal intensity $V \equiv 1$

Visibility

We can define the visibility function as

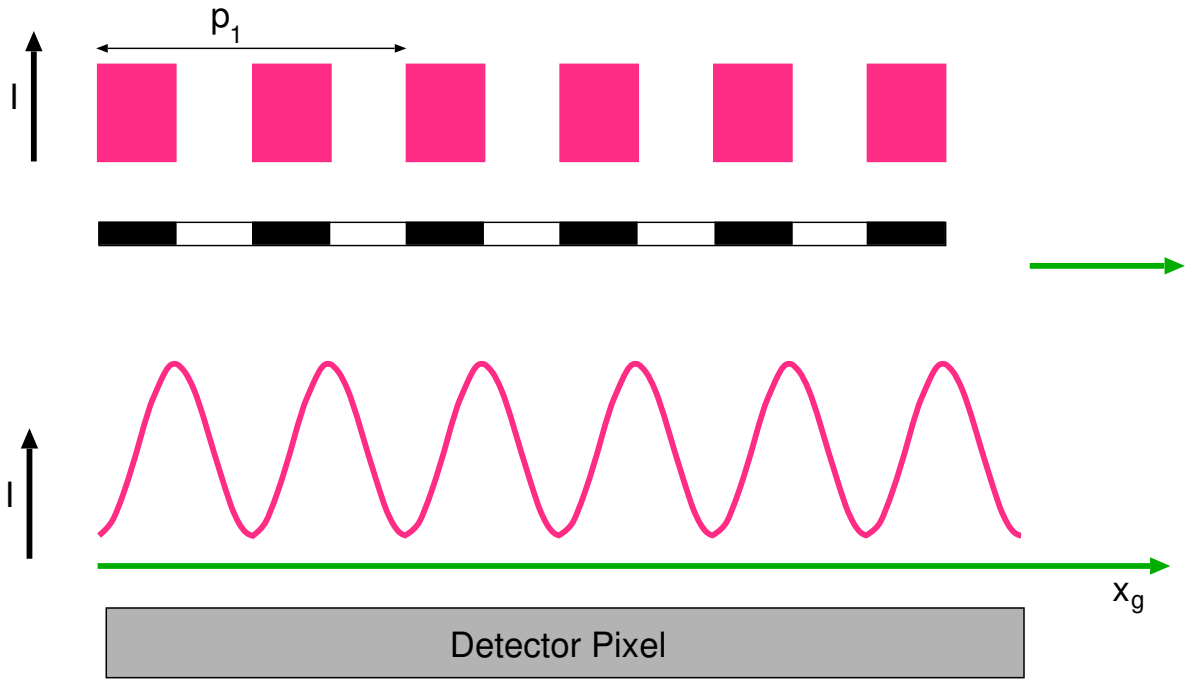

$$V = \frac{I_{max} - I_{min}}{I_{max} + I_{min}}$$

for the ideal intensity $V \equiv 1$ but for small Gaussian smearing, $\sigma \ll p_1$

Visibility

We can define the visibility function as

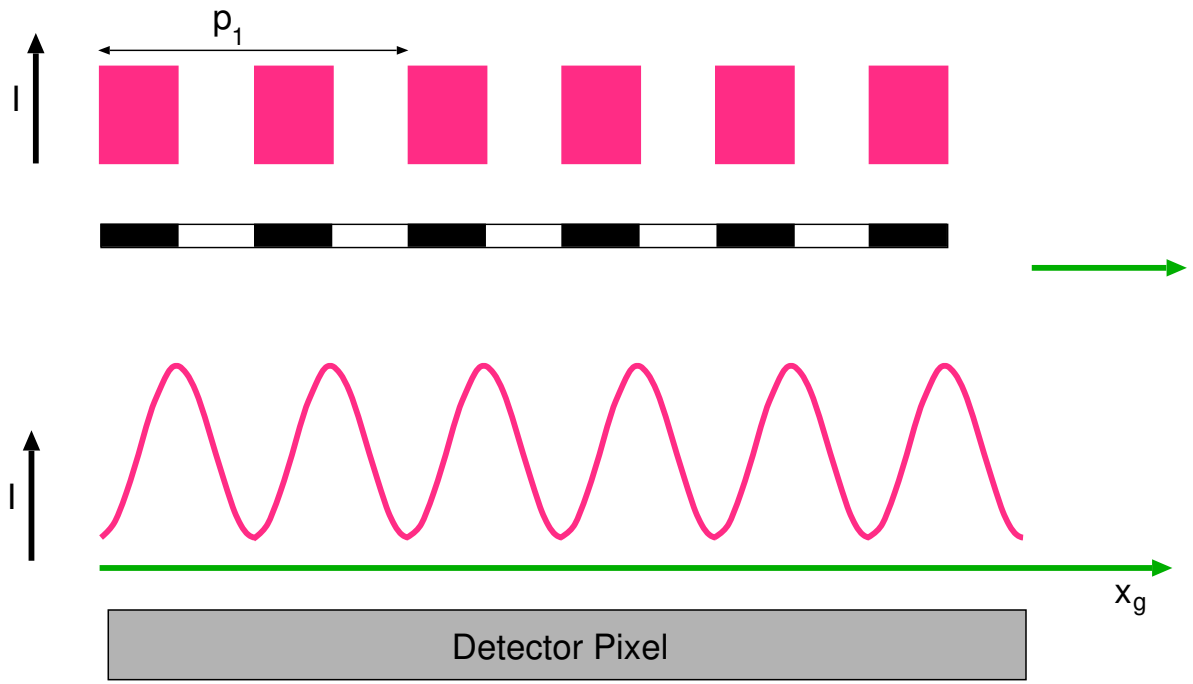

$$V = \frac{I_{max} - I_{min}}{I_{max} + I_{min}}$$

for the ideal intensity $V \equiv 1$ but for small Gaussian smearing, $\sigma \ll p_1$

$$V \approx 1 - \frac{8}{\sqrt{2\pi}} \frac{\sigma}{p_1}$$

Visibility

We can define the visibility function as

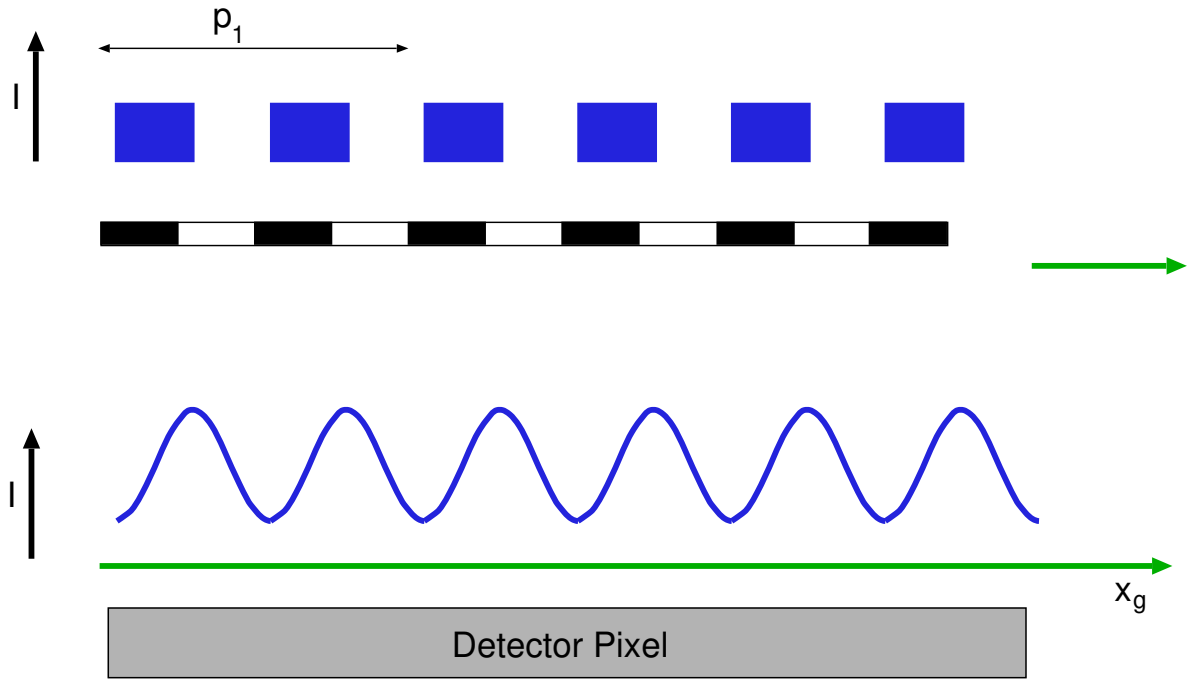

$$V = \frac{I_{max} - I_{min}}{I_{max} + I_{min}}$$

for the ideal intensity $V \equiv 1$ but for small Gaussian smearing, $\sigma \ll p_1$

with the sample in place, the visibility is necessarily smaller due to absorption

$$V \approx 1 - \frac{8}{\sqrt{2\pi}} \frac{\sigma}{p_1}$$

Grating interferometry

Plastic containers filled with water (left) and powdered sugar (right).

(a) absorption image, (b) phase contrast image, (d) dark field image.

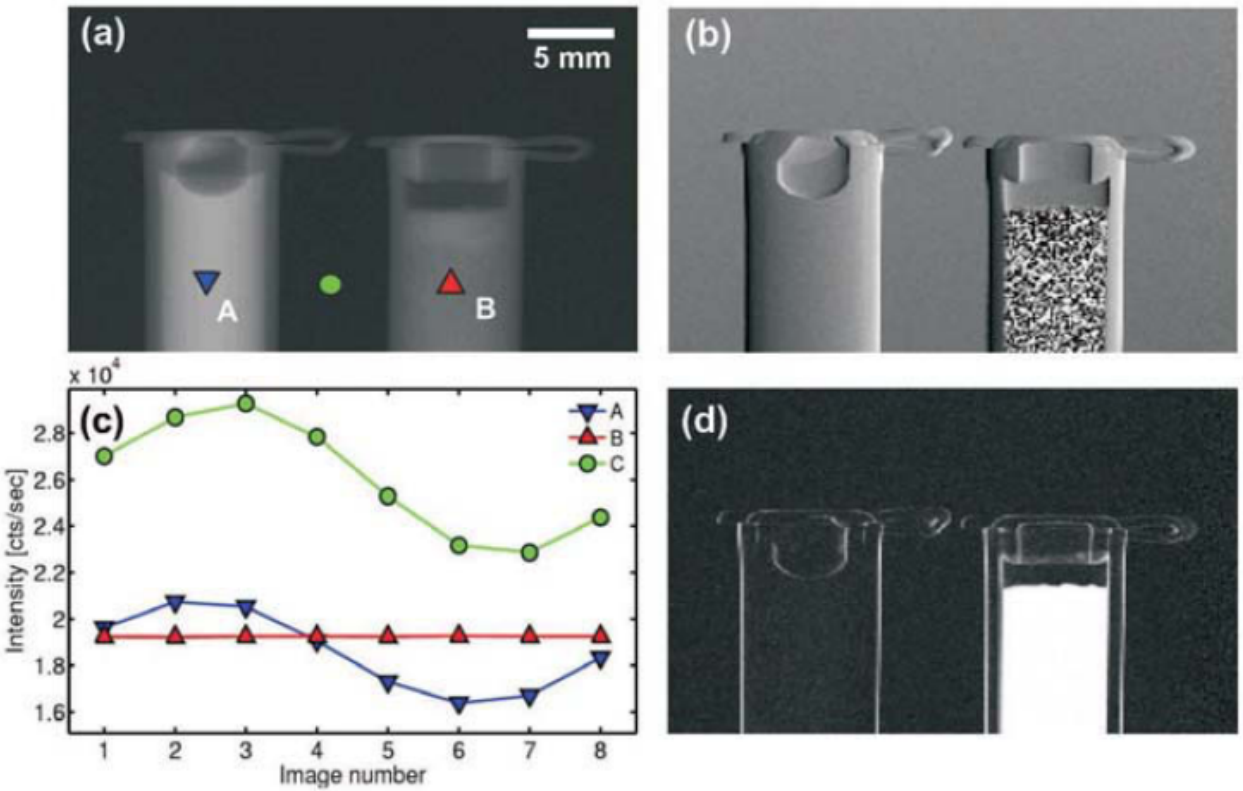

Grating interferometry

Plastic containers filled with water (left) and powdered sugar (right).

(a) absorption image, (b) phase contrast image, (d) dark field image.

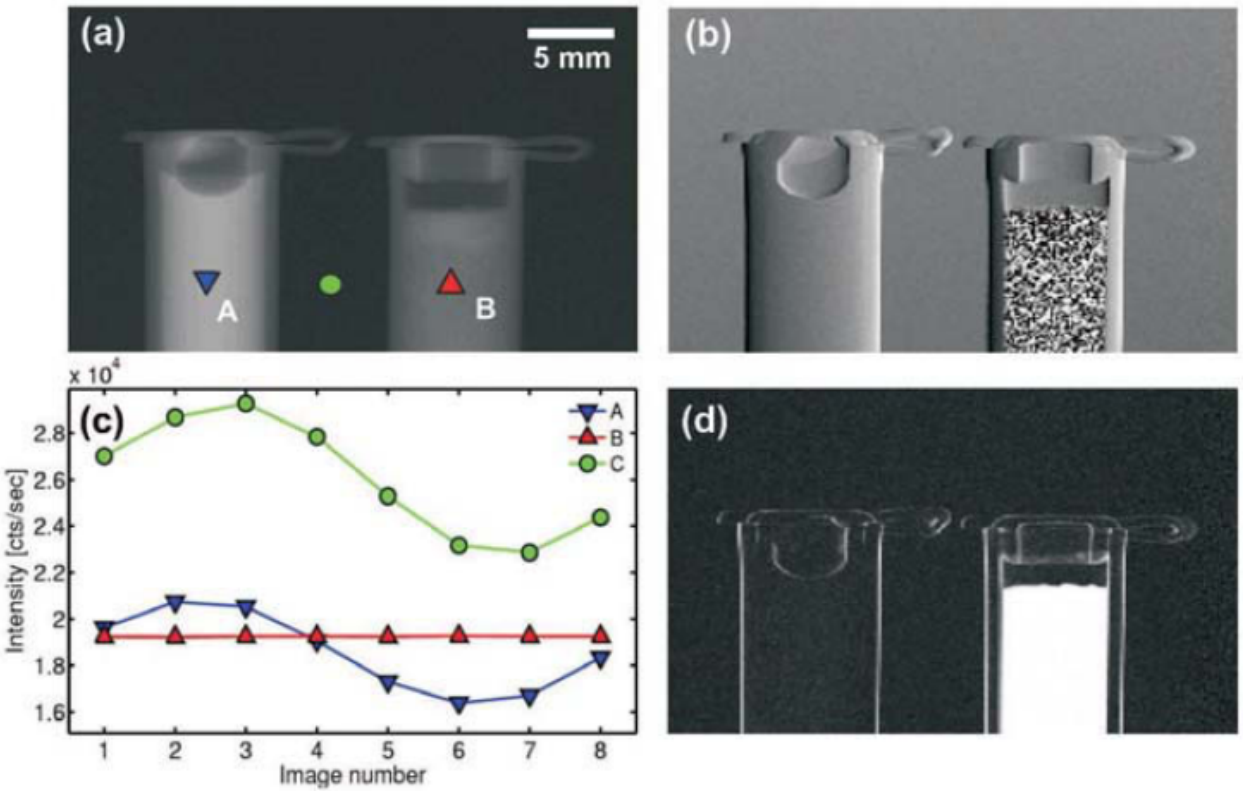

visibility of zero leads to the speckling in (b) as can be seen from the red line in (c)

Grating interferometry

The different contrasts are easily seen in the image of a chicken wing

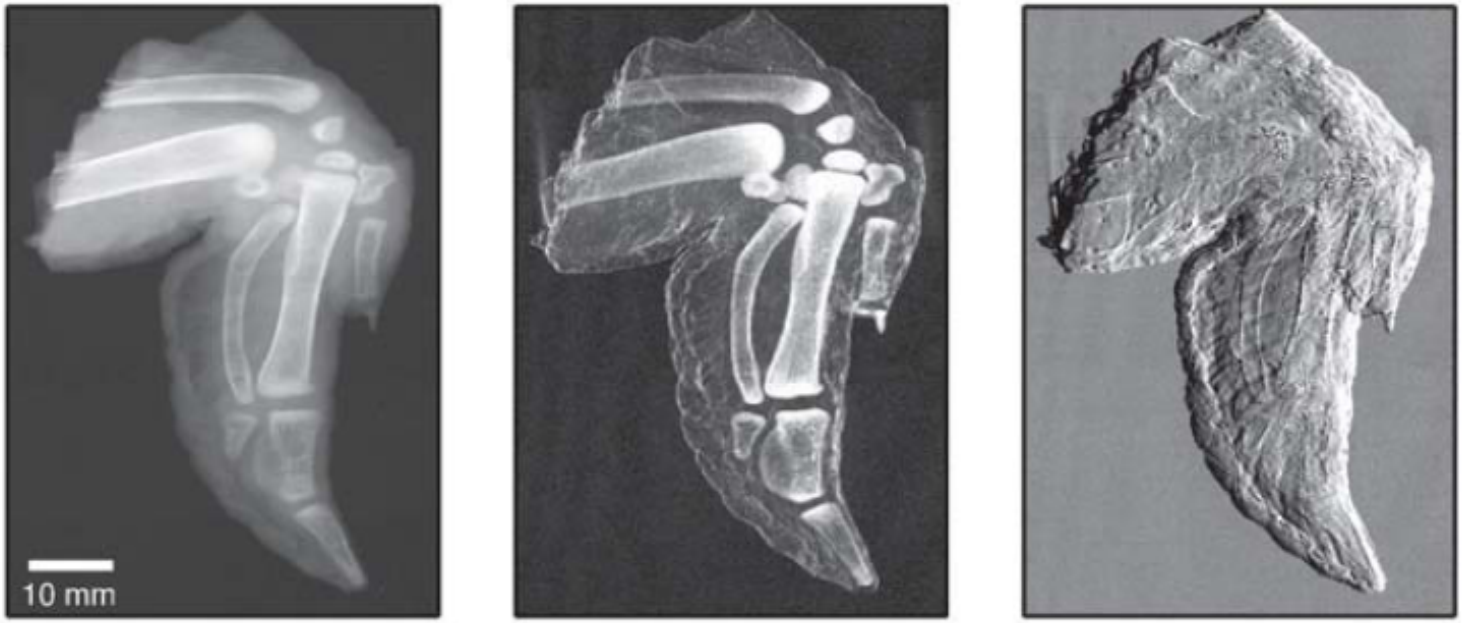

Grating interferometry

The different contrasts are easily seen in the image of a chicken wing

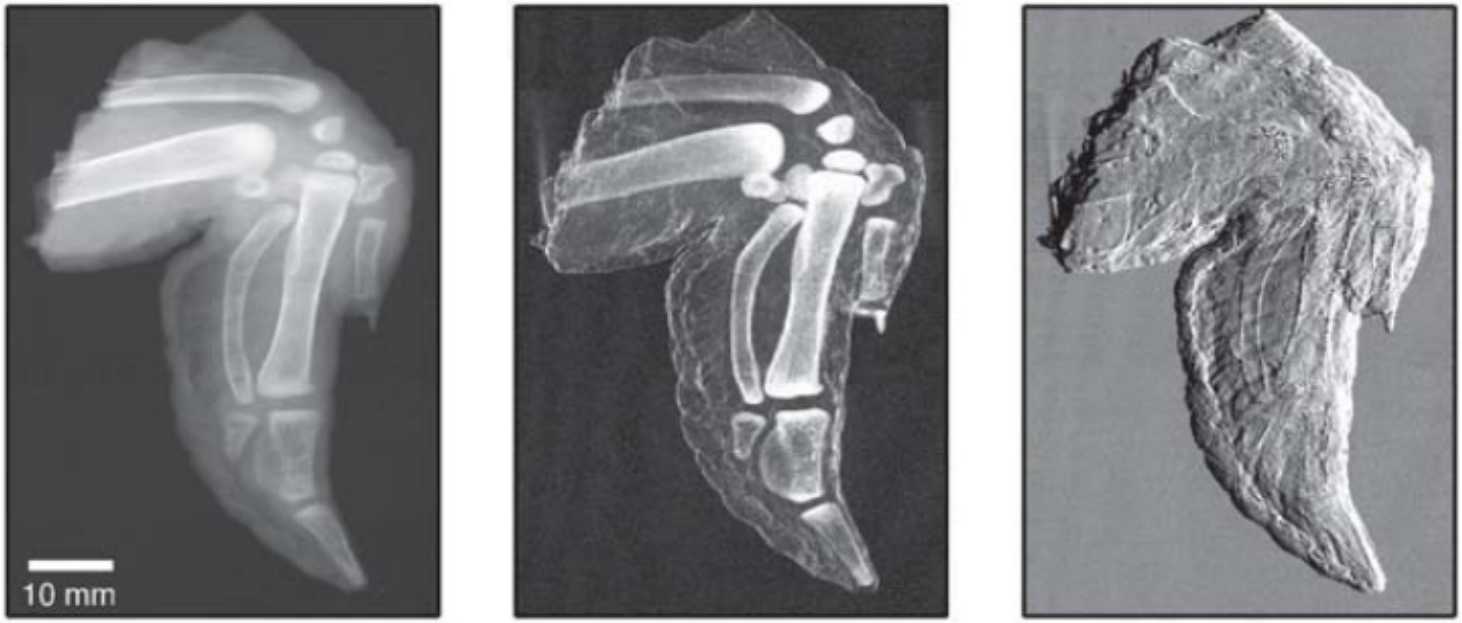

the absorption contrast (left) is most like a conventional radiograph

Grating interferometry

The different contrasts are easily seen in the image of a chicken wing

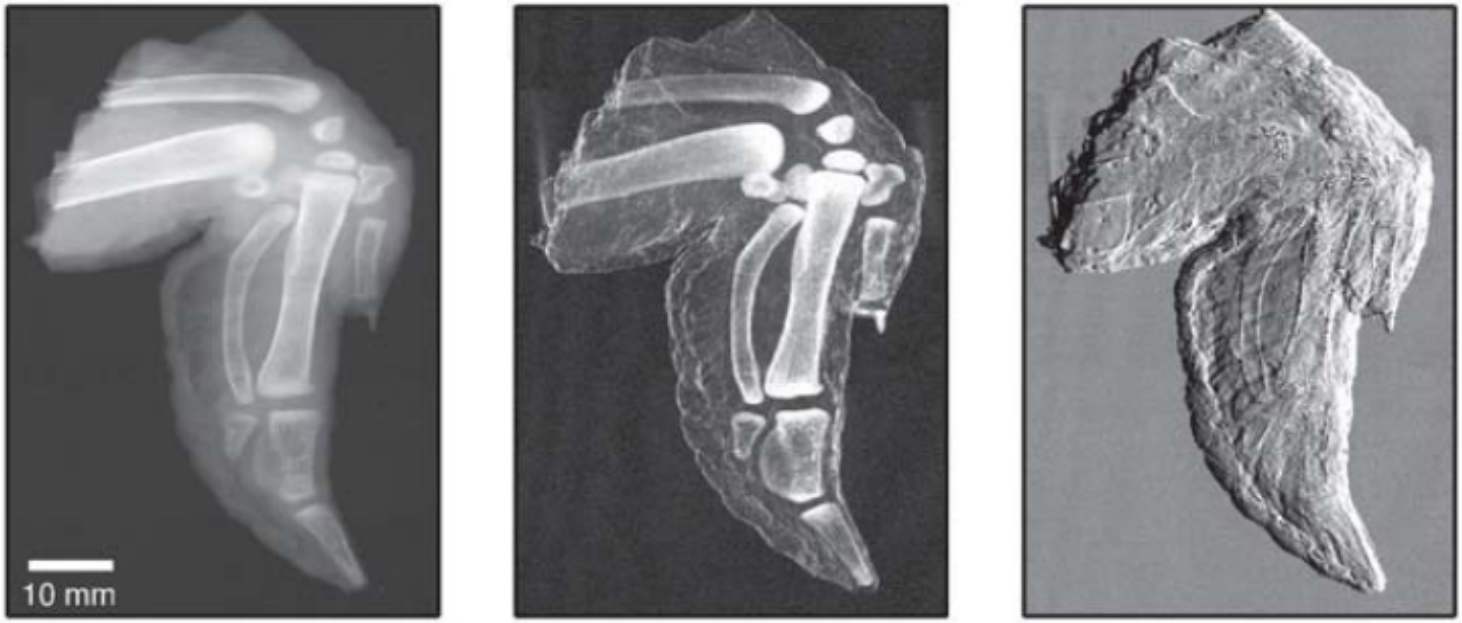

the absorption contrast (left) is most like a conventional radiograph

the phase contrast (right) is sensitive to changes in angle of the surface and buried interfaces

Grating interferometry

The different contrasts are easily seen in the image of a chicken wing

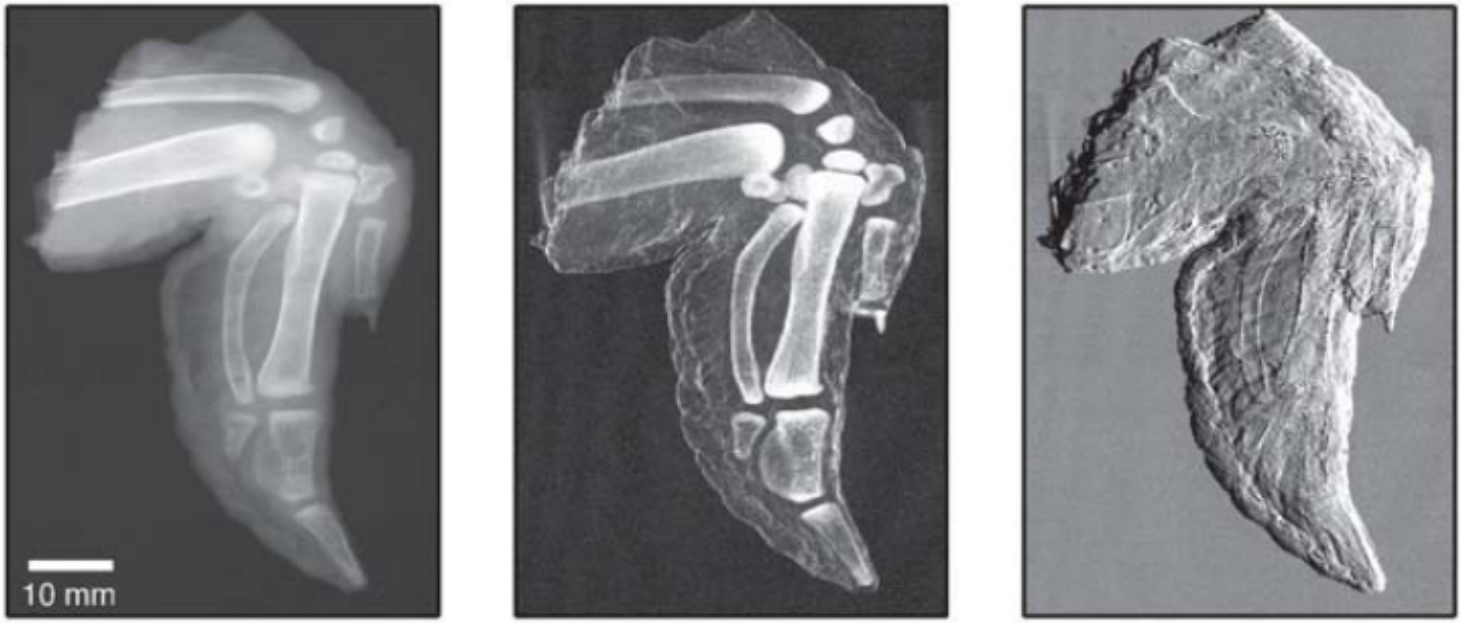

the absorption contrast (left) is most like a conventional radiograph

the phase contrast (right) is sensitive to changes in angle of the surface and buried interfaces

the "dark field" image lights up where there is a a large amount of scattering

Tomography with a Talbot interferometer

The Talbot interferometer may be used for tomography as well

"Phase imaging with an x-ray Talbot interferometer," A. Momose, W. Yashiro, Y. Takeda, Y. Suzuki, and T. Hattora, *JCPDS-International Centre for Diffraction Data*, 21-30 (2006).

Tomography with a Talbot interferometer

The Talbot interferometer may be used for tomography as well

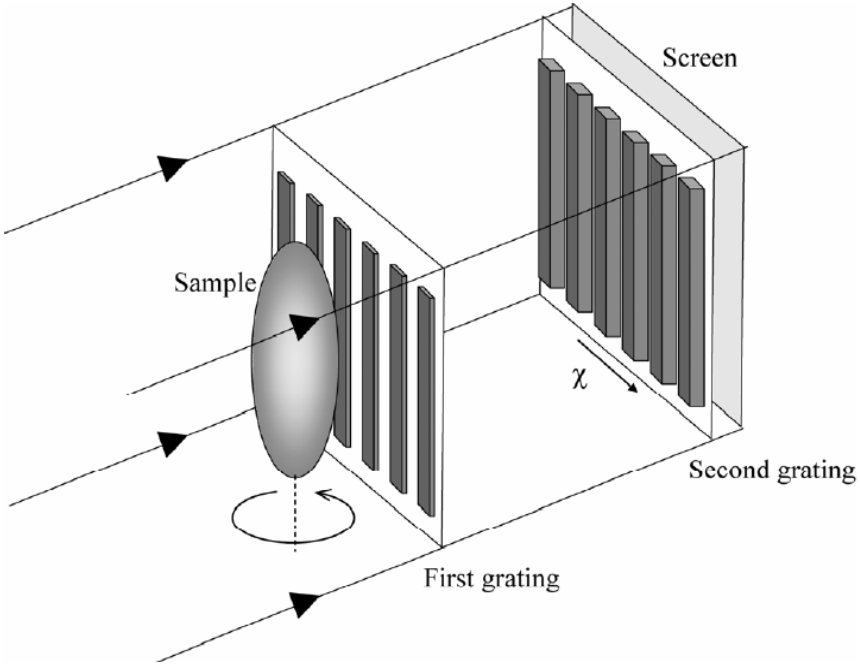

"Phase imaging with an x-ray Talbot interferometer," A. Momose, W. Yashiro, Y. Takeda, Y. Suzuki, and T. Hattora, *JCPDS-International Centre for Diffraction Data*, 21-30 (2006).

Tomography with a Talbot interferometer

The Talbot interferometer may be used for tomography as well

the sample is rotated and the phase data is recorded in the usual way

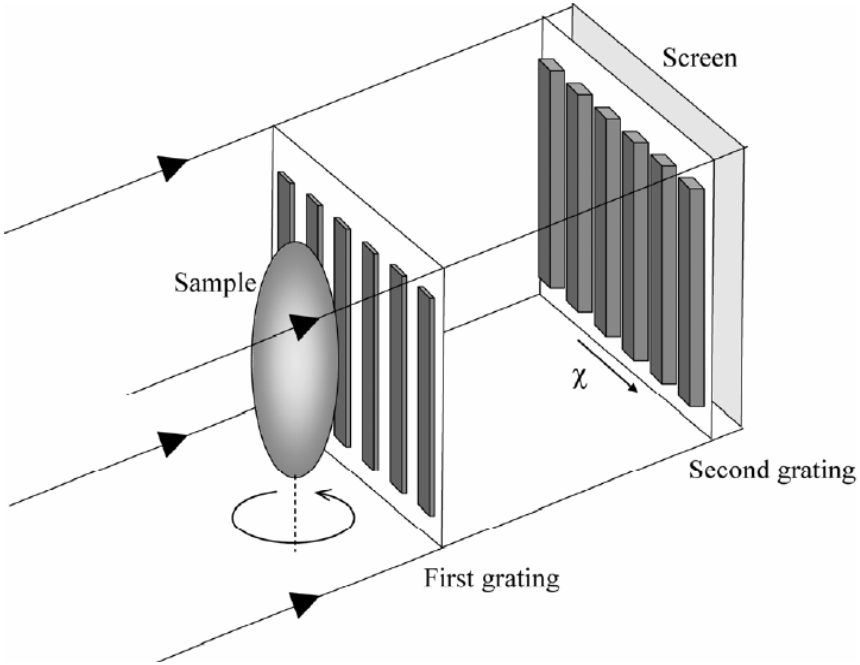

"Phase imaging with an x-ray Talbot interferometer," A. Momose, W. Yashiro, Y. Takeda, Y. Suzuki, and T. Hattora, *JCPDS-International Centre for Diffraction Data*, 21-30 (2006).

Tomography with a Talbot interferometer

The Talbot interferometer may be used for tomography as well

the sample is rotated and the phase data is recorded in the usual way

3D reconstruction was performed on a cancerous rabbit liver

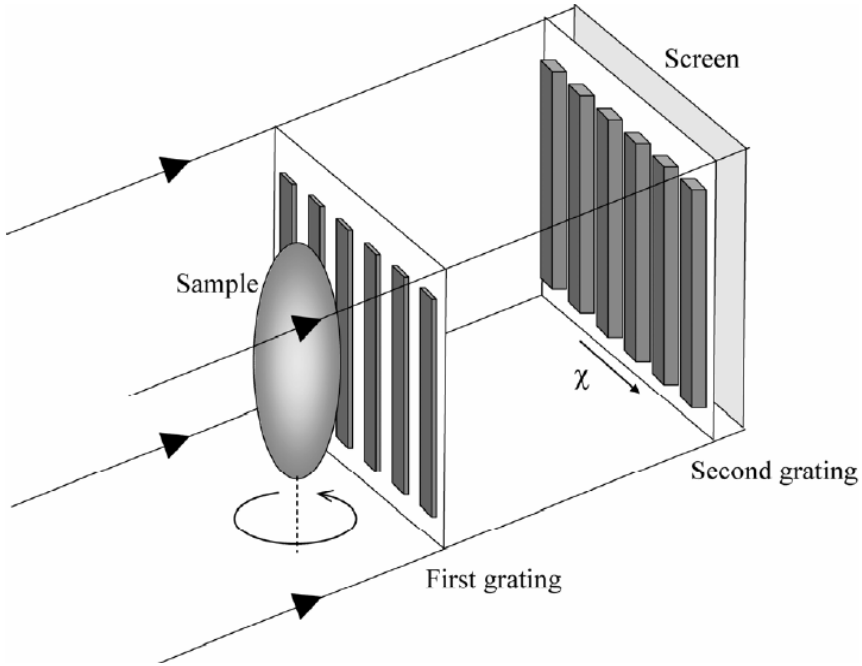

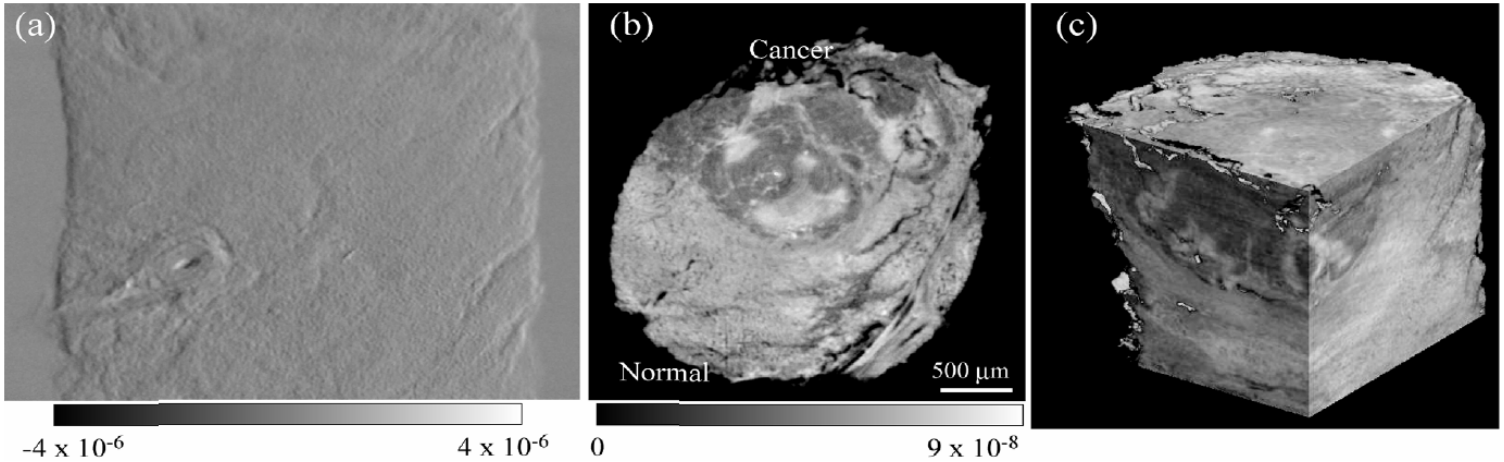

"Phase imaging with an x-ray Talbot interferometer," A. Momose, W. Yashiro, Y. Takeda, Y. Suzuki, and T. Hattora, *JCPDS-International Centre for Diffraction Data*, 21-30 (2006).

Tomography with a Talbot interferometer

The Talbot interferometer may be used for tomography as well

the sample is rotated and the phase data is recorded in the usual way

3D reconstruction was performed on a cancerous rabbit liver then a mouse tail with cartilage and bone

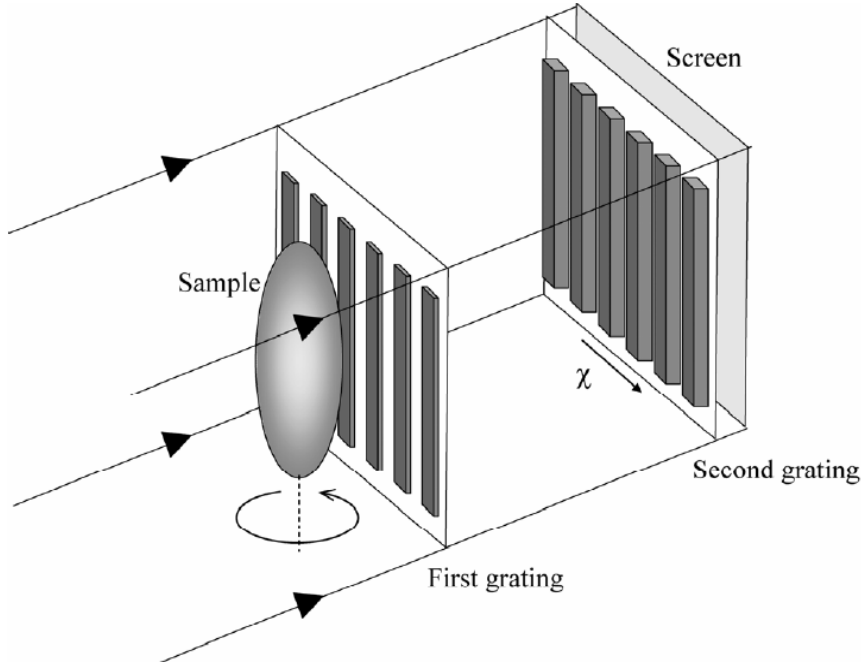

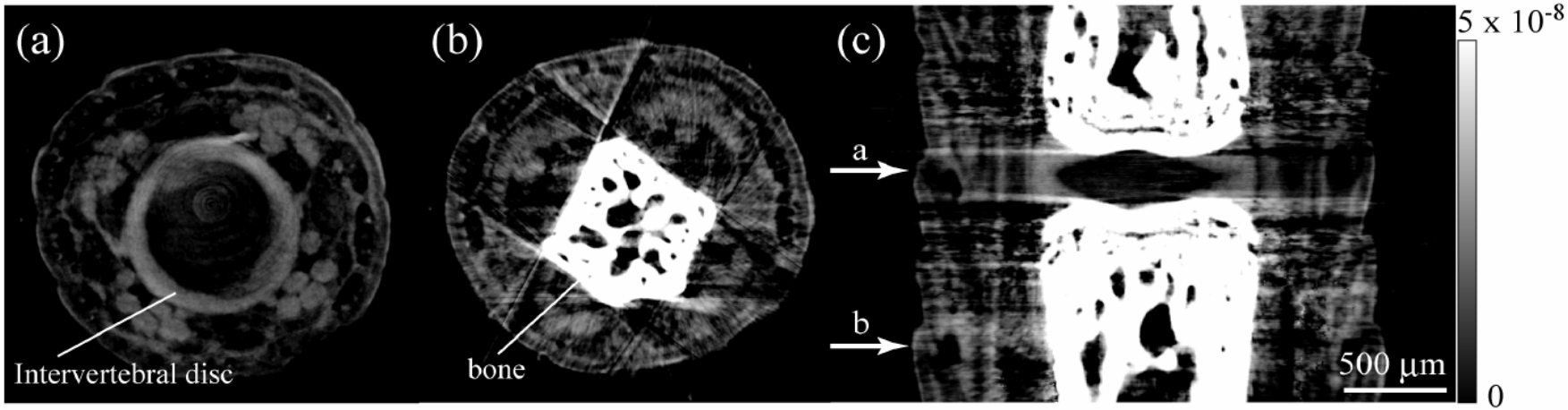

"Phase imaging with an x-ray Talbot interferometer," A. Momose, W. Yashiro, Y. Takeda, Y. Suzuki, and T. Hattora, *JCPDS-International Centre for Diffraction Data*, 21-30 (2006).

SAXS from a sphere

For incoherent beam, illuminating a small particle (a sphere), we have the typical small angle pattern which shows broad features described in a previous chapter

SAXS from a sphere

For incoherent beam, illuminating a small particle (a sphere), we have the typical small angle pattern which shows broad features described in a previous chapter

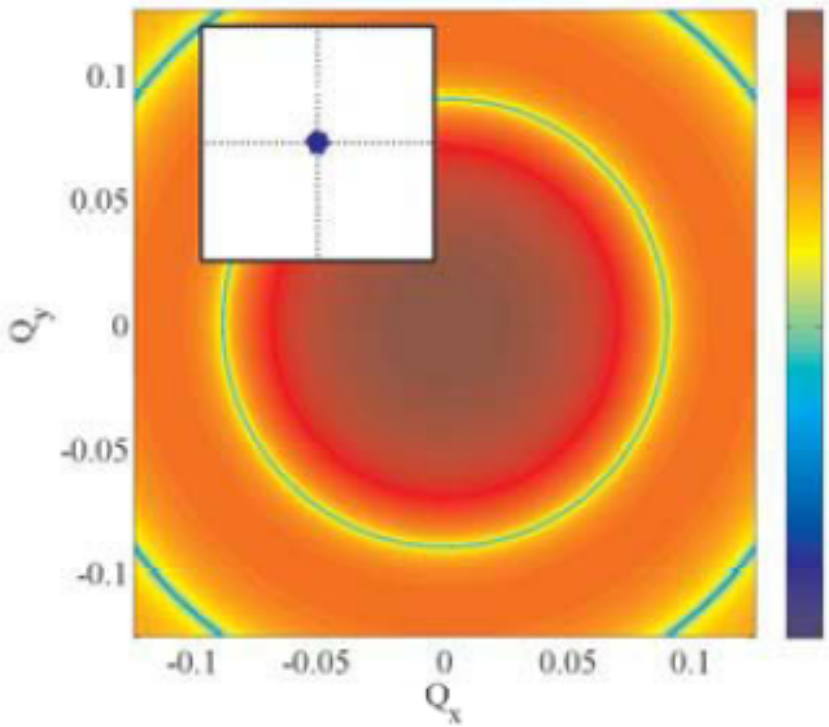

Coherent Scattering from Multiple Spheres

If the beam has coherence at least on the order of the size of the arrangement of the seven spheres shown, one obtains

Coherent Scattering from Multiple Spheres

If the beam has coherence at least on the order of the size of the arrangement of the seven spheres shown, one obtains

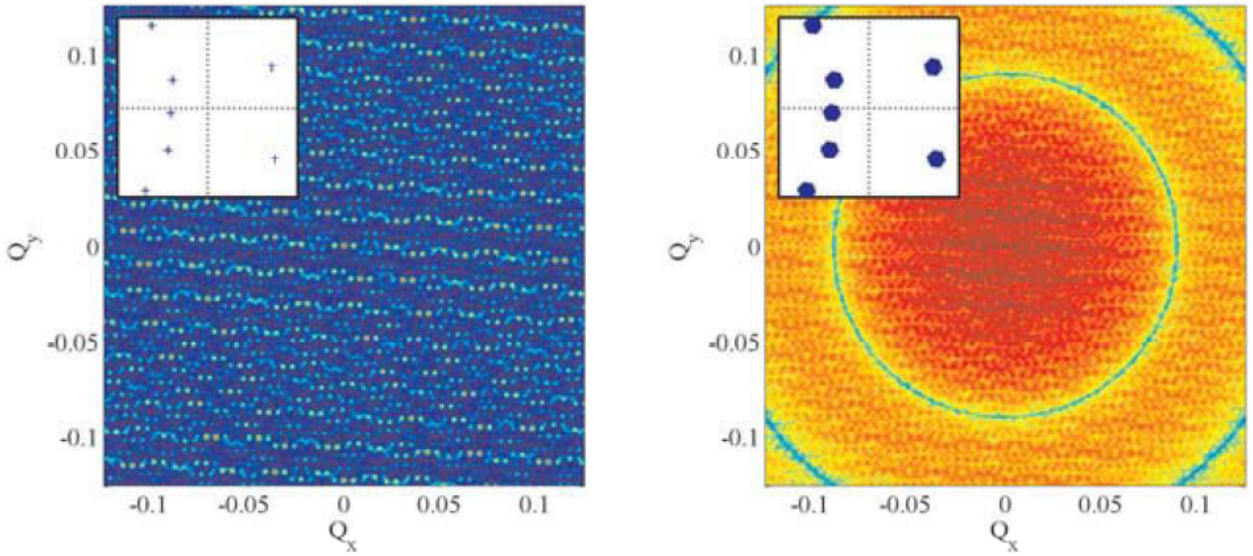

Coherent Scattering from Multiple Spheres

If the beam has coherence at least on the order of the size of the arrangement of the seven spheres shown, one obtains

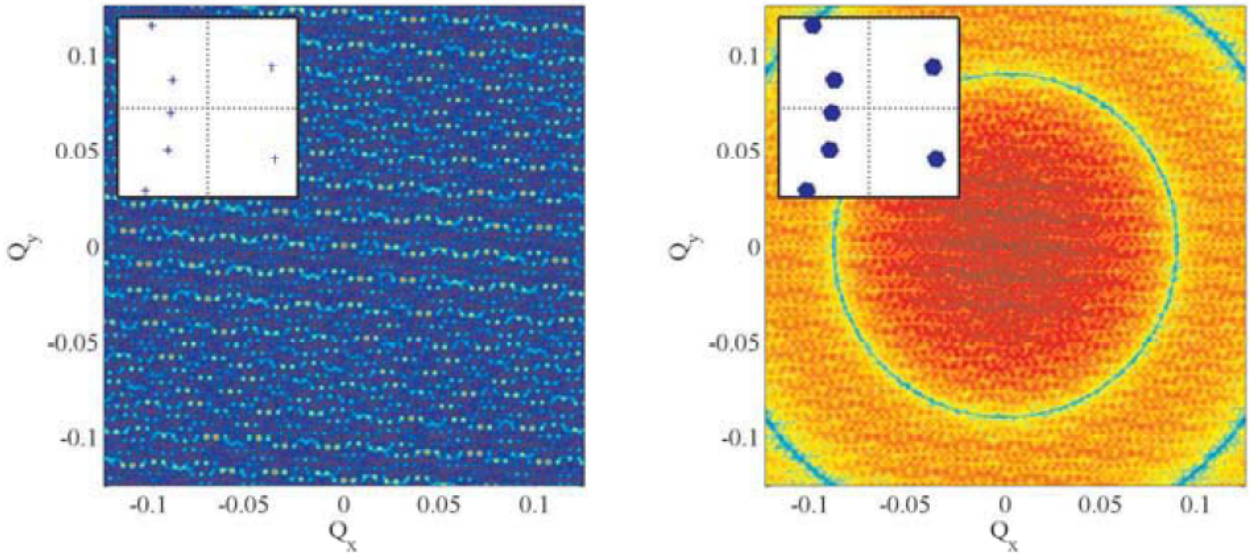

on the left is the "speckle" pattern given by the interference of the coherent beam with the seven spheres,

Coherent Scattering from Multiple Spheres

If the beam has coherence at least on the order of the size of the arrangement of the seven spheres shown, one obtains

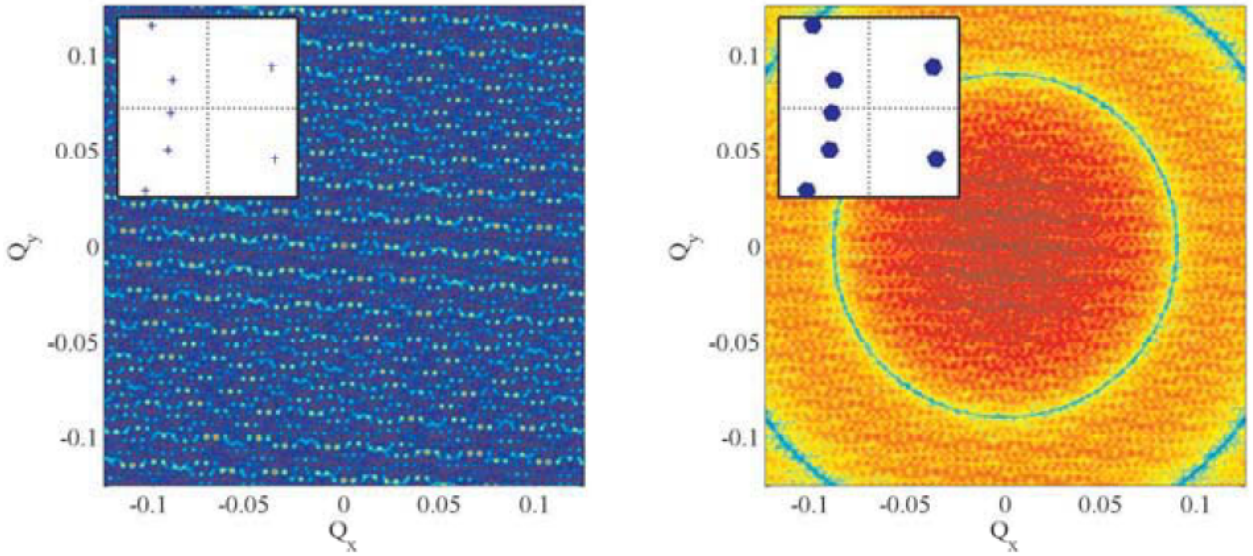

on the left is the "speckle" pattern given by the interference of the coherent beam with the seven spheres, on the right is the full pattern including the SAXS from individual spheres

Coherent Scattering from Multiple Spheres

If the beam has coherence at least on the order of the size of the arrangement of the seven spheres shown, one obtains

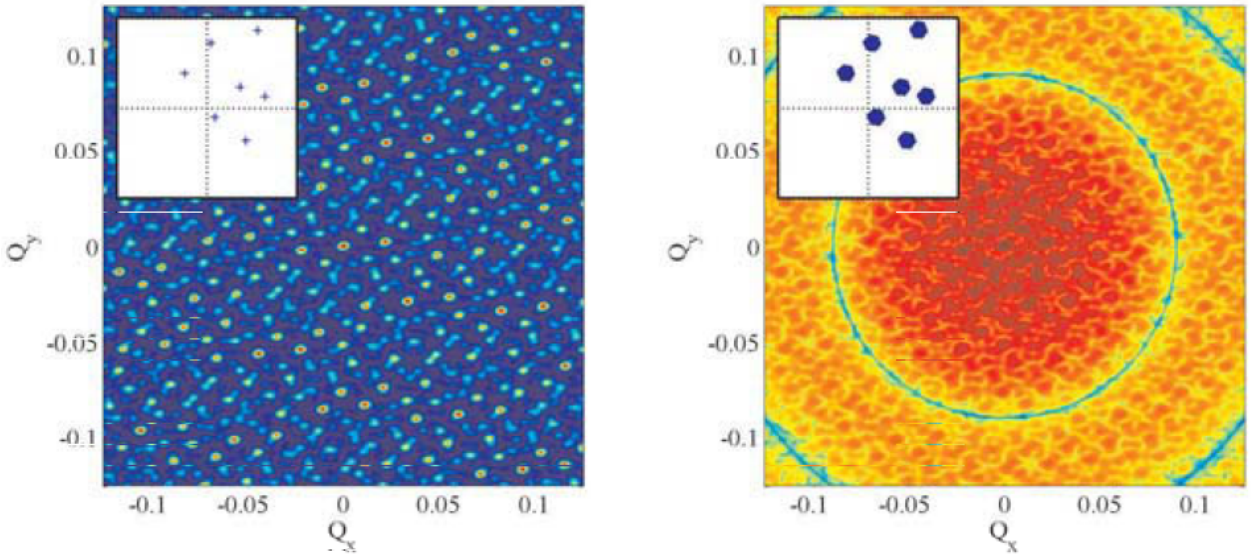

on the left is the "speckle" pattern given by the interference of the coherent beam with the seven spheres, on the right is the full pattern including the SAXS from individual spheres

the speckle changes with a different arrangement of spheres

Coherent Scattering from Multiple Spheres

If the beam has coherence at least on the order of the size of the arrangement of the seven spheres shown, one obtains

T= 295K

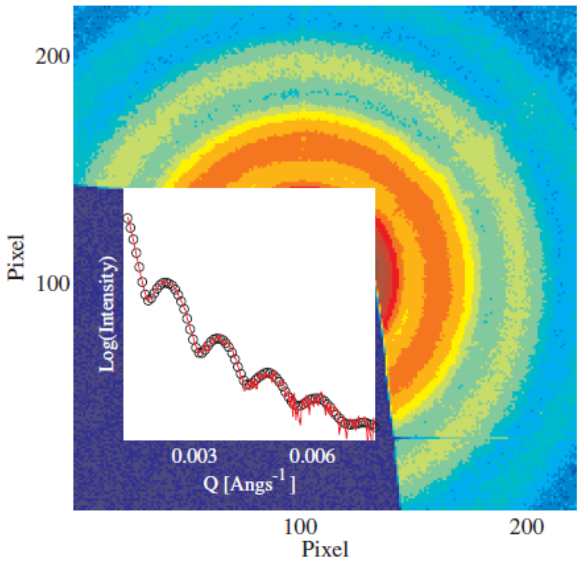

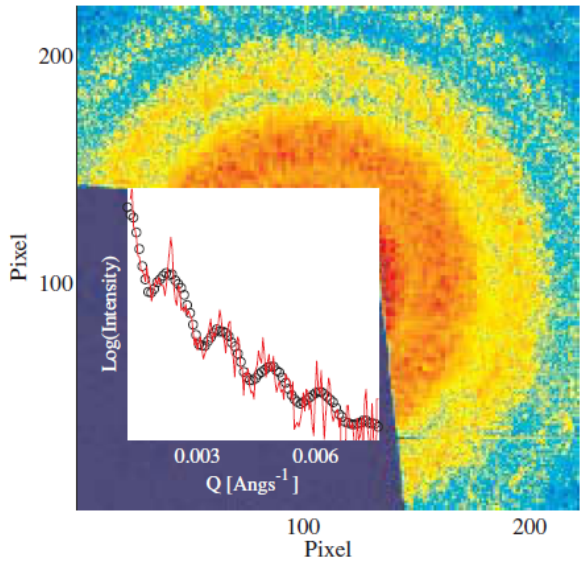

T=145K

on the left is the "speckle" pattern given by the interference of the coherent beam with the seven spheres, on the right is the full pattern including the SAXS from individual spheres

the speckle changes with a different arrangement of spheres

this can be seen when the speckle appears below a glass transition at 145K

Oversampling and image

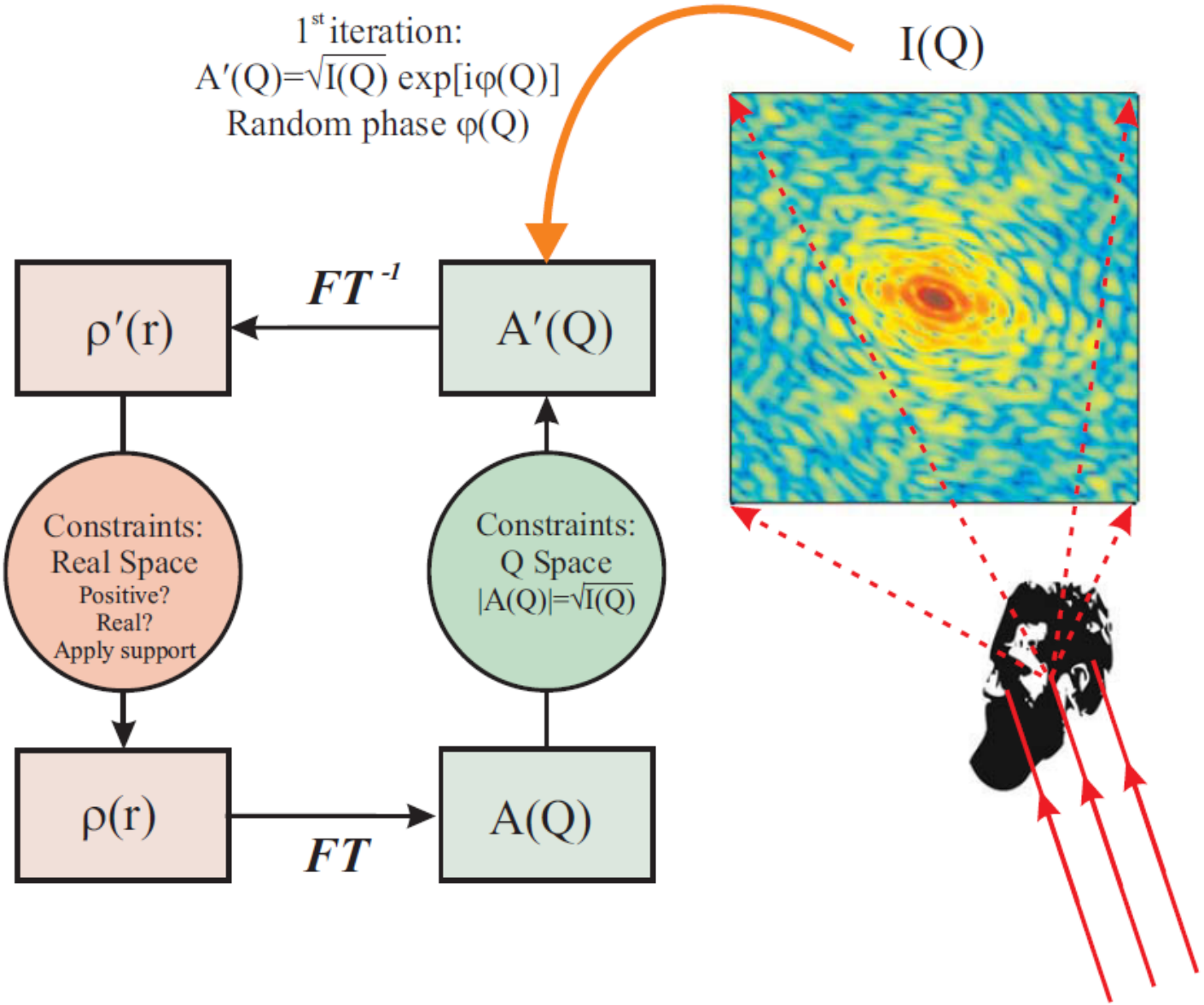

Iterative Reconstruction

start with experimental data and a randomly generated phase

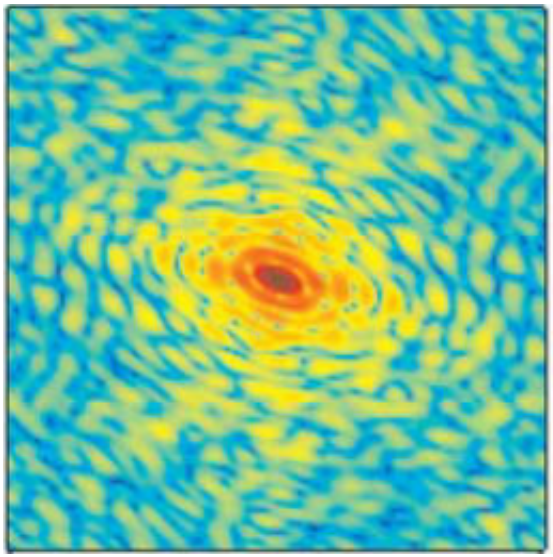

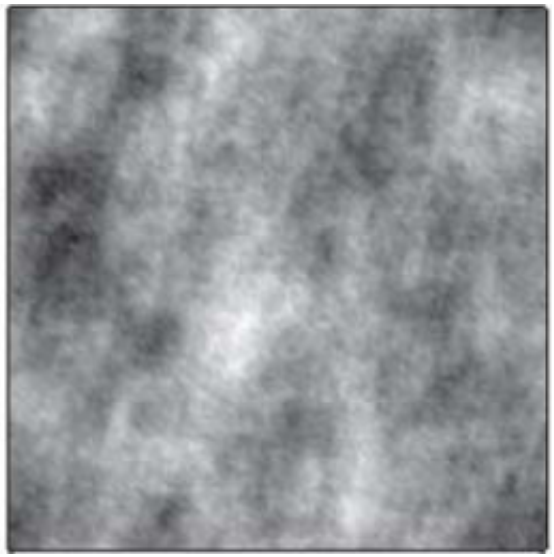

Iterative Reconstruction

start with experimental data and a randomly generated phase

intermediate step shows partial phase retrieval but distorted scattering pattern

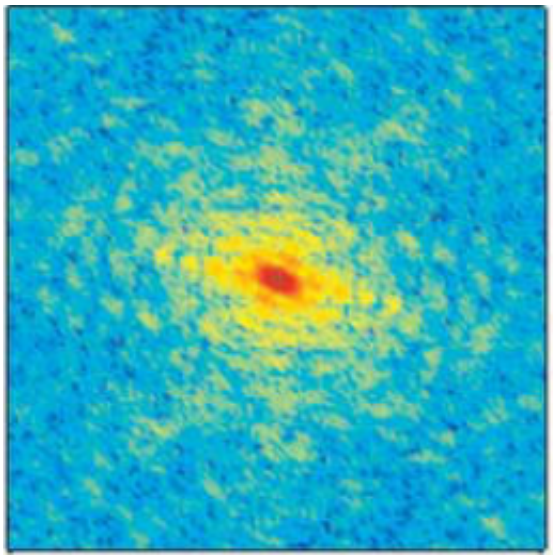
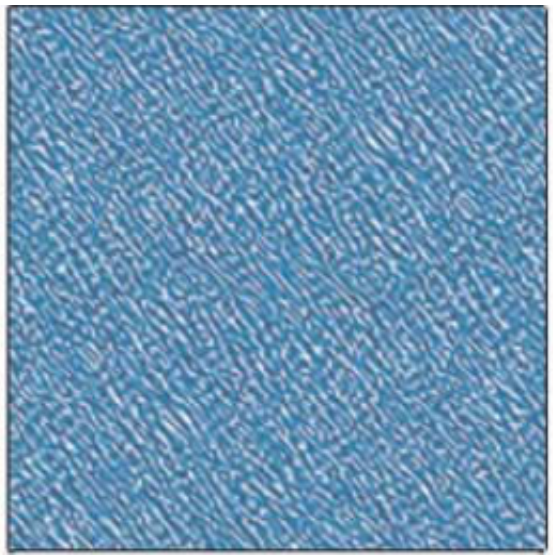


Iterative Reconstruction

start with experimental data and a randomly generated phase

intermediate step shows partial phase retrieval but distorted scattering pattern

convergence to reconstructed phase, scattering and real space image

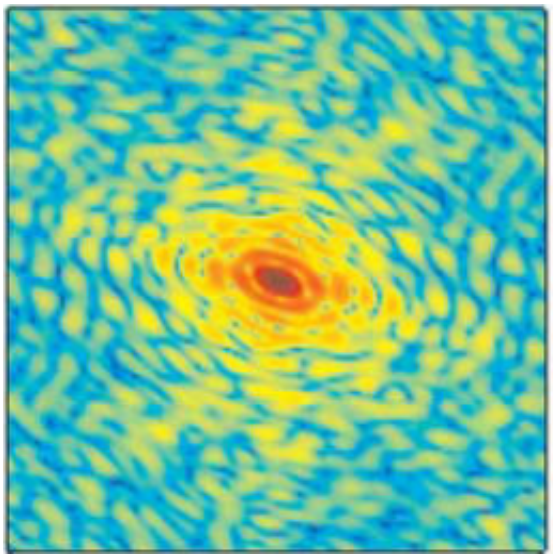

Gold nanoparticle imaging by CXI

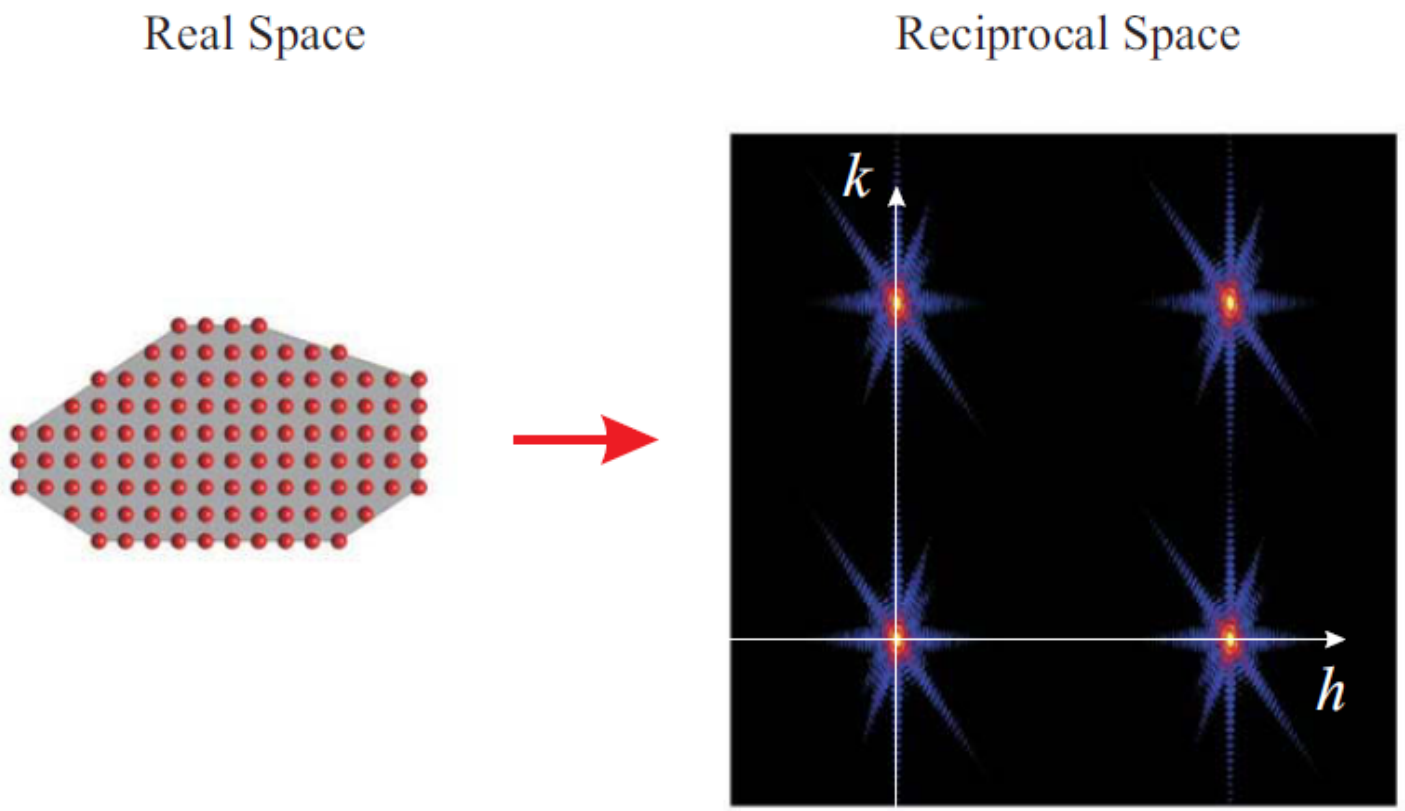

Gold nanoparticle imaging by CXI

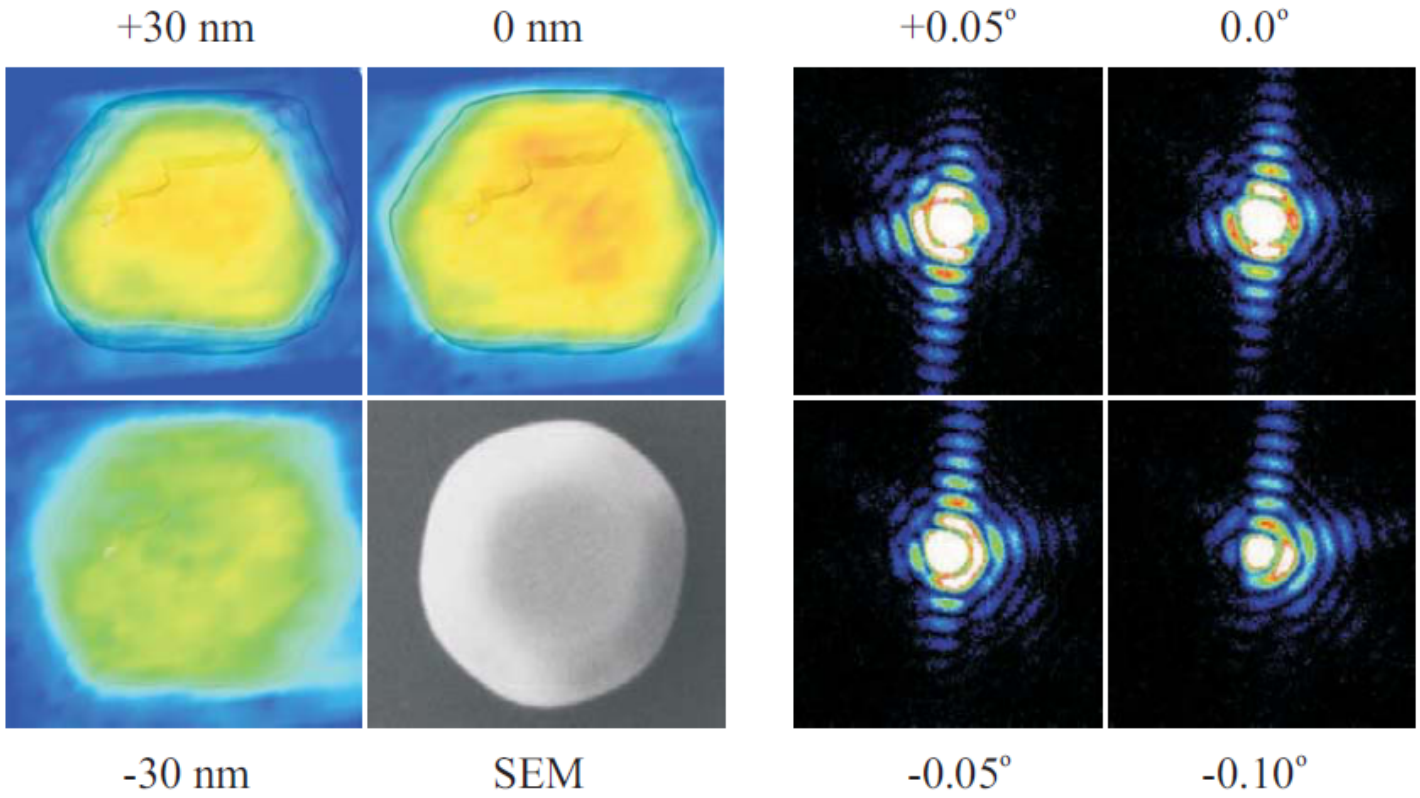

Lattice dynamics by CXI

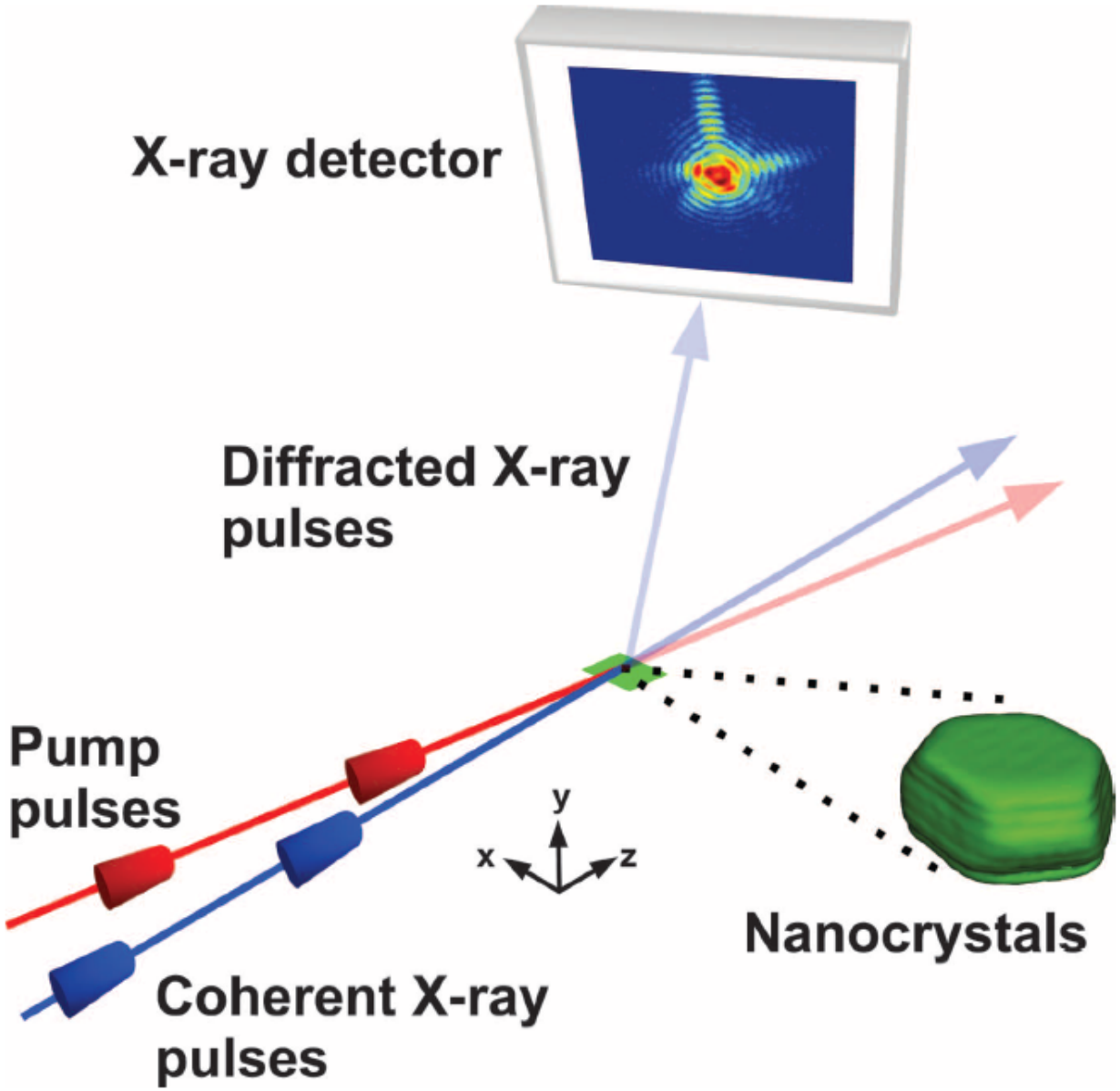

Lattice dynamics by CXI

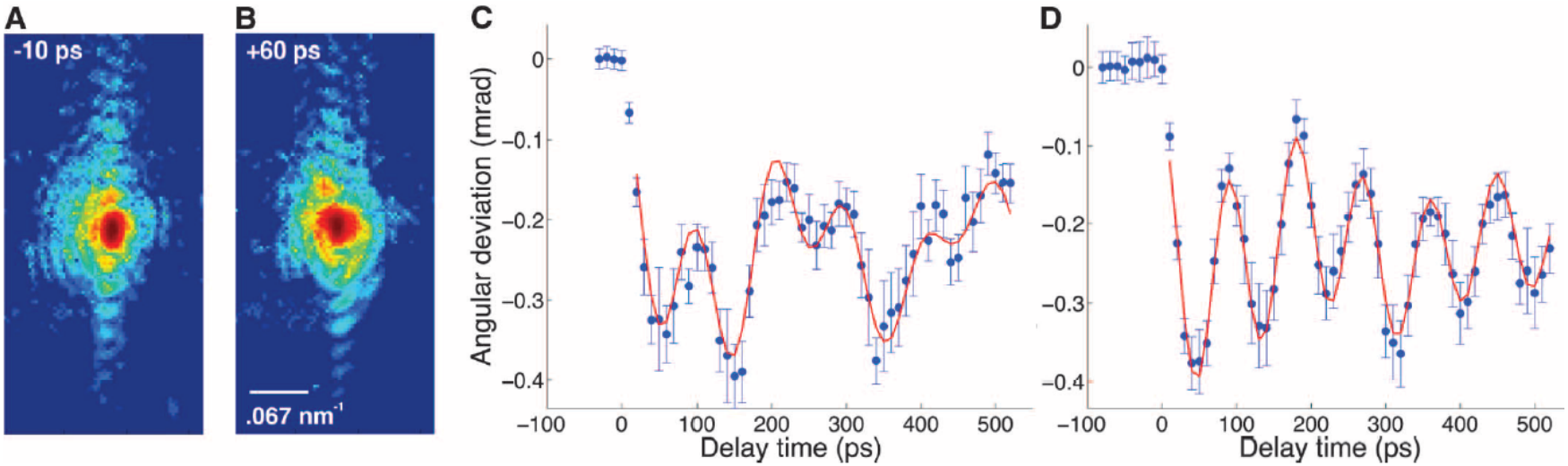

"Ultrafast three-dimensional imaging of lattice dynamics in individual gold nanocrystals," J.N. Clark, et al., *Science* **341**, 56-59 (2013).

Lattice dynamics by CXI

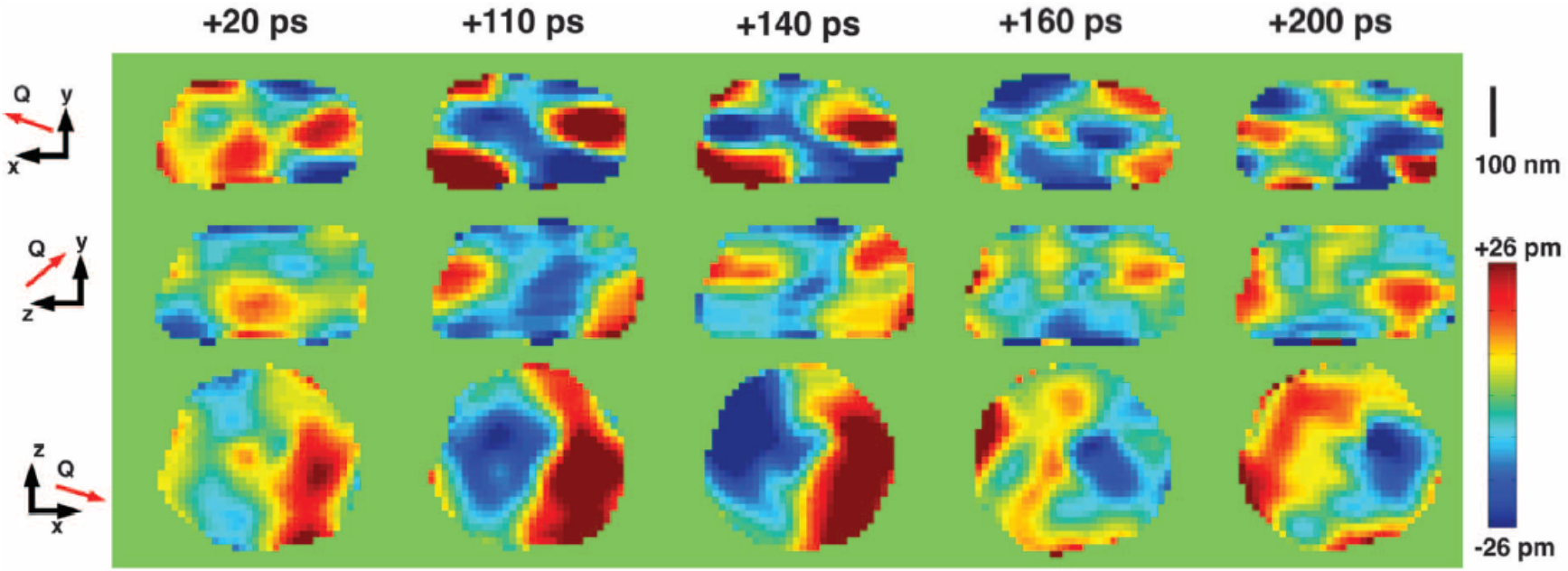

"Ultrafast three-dimensional imaging of lattice dynamics in individual gold nanocrystals," J.N. Clark, et al., *Science* **341**, 56-59 (2013).

Lattice dynamics by CXI

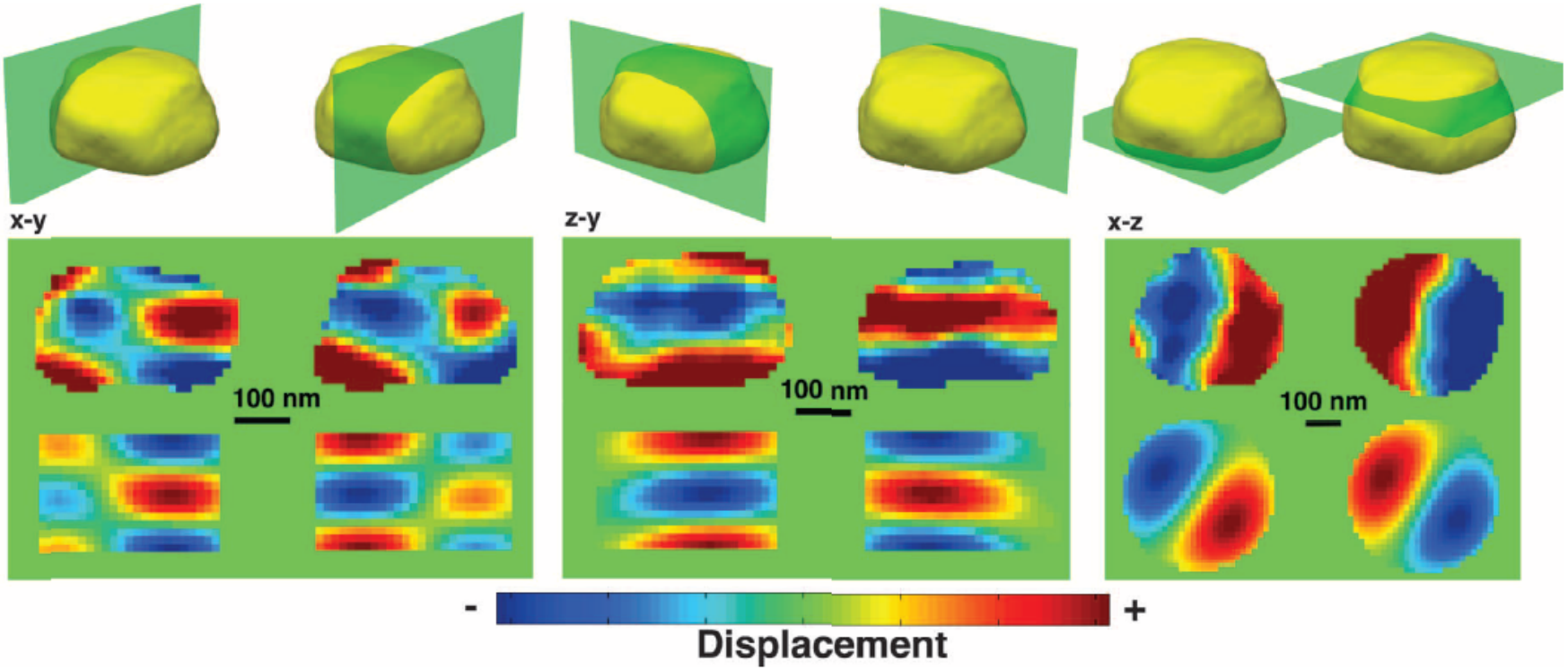

"Ultrafast three-dimensional imaging of lattice dynamics in individual gold nanocrystals," J.N. Clark, et al., *Science* **341**, 56-59 (2013).